The Function and Regulon of Transcription Factor RcsA in *Pantoea* sp. YR343

A Thesis Presented for the
Master of Science
Degree
The University of Tennessee, Knoxville

Grace McSween Satterfield
August 2018

Copyright © 2018 by Grace M. Satterfield
All rights reserved.

ACKNOWLEDGMENTS

Thank you to my supportive and expert advisor, Dr. Jennifer Morrell-Falvey. I would also like to thank the ever-patient and smiling Dr. Amber Bible Webb. In addition, thank you to the Genome Science and Technology Program and the Plant-Microbe Interactions group at Oak Ridge National Lab. Lastly, thanks to my committee, Dr. Sarah Lebeis, Dr. Dale Pelletier, Dr. Todd Reynolds, and Dr. Meg Staton for their contribution to this project and my education.

ABSTRACT

Plants have a microbiome that hosts a variety of microorganisms, including pathogenic, neutral, and beneficial bacterial strains. These strains can influence the plant's growth and health. Determining how the microbiome is recruited and structured and how these microbes communicate and interact with each other is needed to understand, and, ultimately, manipulate the effect of the microbiome on plant health. In order to pursue this goal, we are studying the plant-associated microbe *Pantoea* sp. YR343. *Pantoea* sp. YR343 is a motile and rod-shaped bacterium isolated from the roots of *Populus deltoides*- a promising source for biofuels. It possesses the ability to solubilize phosphate as well as produce the phytohormone indole-3-acetic acid (IAA). Moreover, *Pantoea* sp. YR343 shows both swimming and swarming motility, is a robust root colonizer, and induces lateral root production in *Arabidopsis thaliana* and *Populus deltoides*. As part of a genetic screen to identify factors that promote root colonization, we identified a transposon mutant that mapped to a gene encoding the transcription regulator RcsA. The transposon mutant displayed defects in biofilm formation, capsule production, and colonization of wheat roots, suggesting that it may influence the ability of *Pantoea* sp. YR343 to associate with plants. Understanding the function of this gene in *Pantoea* sp. YR343 provides insights into the regulation and mechanisms of plant association.

TABLE OF CONTENTS

CHAPTER ONE: Background 1
Complex Communities 1
Plant-Microbe Communities 1
Populus deltoides Microbiome 2
Pantoea sp. YR343 4
Colonization and Biofilm Formation of Microbes 5
Exopolysaccharide Production 8
RcsA: Regulator of Capsule Production 9
Regulation of *RcsA* in *Pantoea stewartii* 10
Function of *RcsA* in *Pantoea stewartii* 11
CHAPTER TWO: The Function and Regulon of Transcription Factor RcsA in *Pantoea* sp. YR343 15
Selecting RcsA 15
Methods 17
Results 18
Discussion and Future Directions 31
CHAPTER THREE: Other Projects 33
LuxR: A Master Regulator 34
LrhA: A Transcription Factor 36
Symplasmata 38
The Mysterious BB4 Transposon Mutant: A DNA Helicase 43
C-di-GMP-related Transposon Mutants 45
Salicin Degradation 48
Transport Transposon Mutants 52
List of References 58
Appendix 63
Progress with the *rcsA* and *lrhA* Clean Deletions 64
Primers 66
Vita 68

LIST OF TABLES

Table 2.1. Genes downregulated in *rcsA:*Tn5 compared to WT *Pantoea* sp. YR343. grown overnight in R2A media. We generated the expression matrix using DESeq2 in KBase and filtered with a log2_fold_change cutoff of 2 and q-value (corrected p-value) of 0.05……..……27

Table 2.2. Genes upregulated in *rcsA:*Tn5 compared to WT *Pantoea* sp. YR343. grown overnight in R2A media. We generated the expression matrix using DESeq2 in KBase and filtered with a log2_fold_change cutoff of 2 and q-value (corrected p-value) of 0.05……..……28

Table 3.1. BLAST ID and number of LuxR homologs in *Pantoea* strains compared to *Pantoea* sp. YR343 34

Table 3.2. BLAST ID and number of LuxI homologs in *Pantoea* strains compared to *Pantoea* sp. YR343 (PMI39_00509) ……35

Table 3.3. ATP/OD readings show no significant differences. Testing the supernatant alone rendered no ATP reading, so salicylate does not contribute to the results..... 51

Table 3.4. Overview of transport mutants isolated from c-di-GMP transposon screen. "-" indicates no significant phenotypic difference from the WT. 53

Table 3.5. Predicting the function of transport mutants isolated from c-di-GMP transposon screen. 54

Table 3.6. Summary of proteomics for *Pantoea* sp. YR343 transport mutants. 56

Table 3.7. Summary of crytal violet biofilm assay for *Pantoea* sp. YR343 transport mutants. ... 57

Table A.1. Primers. 66

LIST OF FIGURES

Figure 1.1. Beneficial plant-microbe interactions in the rhizosphere. 1) Motility, 2) Adherence, and 3) Growth are the essential steps to compete in the rhizosphere. PGPR strains can release nutrients and phytohormones as well as inhibit root diseases caused by pathogens by 4) causing the plant to elicit Induced Systemic Resistance (ISR) or 5) directly producing secondary metabolites.[3] 3

Figure 1.2. Hybrid poplars planted like row crops. Can be processed into ethanol as alternative fuel.[1] 4

Figure 1.3. *Pantoea* sp. YR343 colonizing *Populus deltoides*. *Populus deltoides* WV94 cuttings grown in presence or absence of *Pantoea* YR343 expressing GFP for seven days. We detected plant roots using red autofluorescence and YR343 using GFP (green fluorescent protein) fluorescence. 7

Figure 1.4. Quorum sensing and biofilms. a. Steps involved in biofilm development. b. Confocal microscope images of P. aeruginosa developing a biofilm over time while producing GFP. The tower structures after 8 days are 100 um high.[6] 7

Figure 1.5. Symbiotic bioluminescence as a result of lux-gene organization. b. Australian pinecone fish has a lower light organ on the haw that contants ~10^10 *V. fischeri* cells per ml fluid. Pinecone fish use the light to search for prey at night. c. Hawaiian bobtail squid with an organ with ~10^11 *V. fischeri* cells per ml close to the ink sac. Bobtail squids emit light downward to blend with the moon and starlight to become invisible to predators.[6] 7

Figure 1.6. Physiological functions and structure of c-di-GMP. c-di-GMP is controlled by diguanylate cyclases that carry GGDEF (red) domains and specific phosphodiesterases that carry EAL or HD-GYP domains (blue). c-di-GMP can reduce motility by downregulating flagellar expression or interfering with flagellar motor function. High c-di-GMP levels stimulate biofilm-associate functions, like the formation of fimbriae and other adhesins and various matrix EPS.[7] 8

Figure 1.7. Signal transduction pathway for RcsA, B, C, and D genes. Phosphate transfer from RcsC to RcsB is shown. HNS negatively regulates *rcsA* transcription.[5] 10

Figure 1.8. Regulation of *lrhA* and *rcsA* in *Pantoea stewartii*. At high cell densities, EsaR forms a complex with AHL and becomes inactivated. It cannot bind to the DNA or coordinate the

expression of genes. At low cell densities, EsaR is free to bind to its recognition site and coordinate the expression of genes, like *lrhA* and *rcsA*. 12
Figure 1.9. RcsA and Lrha in Pantoea stewartii. A. Capsule assay showing reduced capsule in RcsA knock-out mutant (center) compared to WT (left). Recovered capsule in complementation (right). B. Swarming assay showing reduced swarming in LrhA knock-out (center) compared to WT (left) and complementation (right). C. Regulatory model of RcsA and LrhA.[2] 13
Figure 1.10. Phylogenetic tree of *Pantoea* YR343 with other *Enterobacteriaceae* species..... 16
Figure 2.1. WT and *rcsA:*Tn5 on Congo Red plates (top) v. overexpressing c-di-GMP with induction of IPTG on Congo Red plates (bottom). 16
Figure 2.2. RcsA sequence with known domains created by BLASTp. Transposon enters at base pair 18. 16
Figure 2.3. RcsA promotes EPS production. A. Congo Red Phenotypes. B. Capsule Analysis... 20
Figure 2.4. Monosaccharide analysis of *rcsA:*Tn5 and *UDP:*Tn5 compared to WT…… 21
Figure 2.5. Gene neighborhood of *UDP* in *Pantoea* sp. YR343, *Erwinia amylovora,* and *Pantoea stewartii*……....21
Figure 2.6. Pellicle formation of WT and mutants in *Pantoea* sp. YR343…… 22
Figure 2.7. Crystal violet biofilm assay shows decreased biofilm formation for *rcsA:*Tn5 mutants compared to WT and pSRK:*rcsA*……..…… 23
Figure 2.8. Colonization of *rcsA*:Tn5 and WT on individual wheat roots…… 24
Figure 2.9. Colonization of *rcsA*:Tn5 and WT inoculated on the same wheat roots……..…...24
Figure 2.10. pPROBE:*rcsA*_promoter expressing GFP ……..……..26
Figure 2.11. A. pPROBE:*UDP*_promoter in WT background and pPROBE:*UDP*_promoter in *rcsA:*Tn5 background …….....26
Figure 2.12. Heatmap of gene functions upregulated in the *rcsA:*Tn5 mutant compared to WT *Pantoea* sp. YR343 grown as pellicles. Darker colors correlate with increased number of genes with predicted COGs in each category. Category key is in Figure 2.14. ……29
Figure 2.13. Heatmap of gene functions downregulated in the *rcsA:*Tn5 mutant compared to WT *Pantoea* sp. YR343 grown as pellicles. Darker colors correlate with increased number of genes with predicted COGs in each category. Category key is in Figure 2.14. ……29

Figure 2.14. Category key for heatmap of predicted COG functions in Figures 2.12-13…..…..30
Figure 3.1. LuxR likely positively regulates LrhA and negatively regulates RcsA in *Pantoea* sp. YR343. In turn, LrhA suppresses genes with motility functions and RcsA activates genes that produce EPS, like UDP. In addition, both LrhA and RcsA contribute to the development of symplasmata.....33
Figure 3.2. Gene neighborhood of LuxR adjacent to LuxI (PMI39_00508) in *Pantoea* sp. YR343……34
Figure 3.3. Colonization of *rcsA:*Tn5, *lrhA:*Tn5, and *luxR:*Tn5 inoculated with WT *Pantoea* sp. YR343 on wheat roots.....35
Figure 3.4. Colonization of *rcsA:*Tn5, *lrhA:*Tn5, and *luxR:*Tn5 inoculated on individual wheat roots.....36
Figure 3.5. A. BLASTp tree of transcription factor LrhA in *Pantoea* sp. YR343. B. BLASTp top hits for RcsA and LrhA in *Pantoea* sp. YR343. Yellow arrow indicates the location of the *Pantoea stewartii* LrhA homolog in the BLASTp tree.....37
Figure 3.6. LrhA phenotypes. A. Swarming assay of WT, LrhA:Tn5, pSRK:LrhA. B. Crystal violet biofilm assay. 38
Figure 3.7. *Pantoea eucalypti* 299R form symplasmata. A. Phase-contrast image showing pair of symplasmata (top). Counter-staining with Indian ink reveals capsule surrounding cells (bottom). B. Cells expressing either GFP or DsRed depicting clonal tendency of symplasmata. Bar = 20 um.[4].....39
Figure 3.8. *Pantoea* sp. YR343 form symplasmata. A. Pellicles contain abundant symplasmata. Brightfield image of symplasmata of various sizes. B. Symplasmata formation on wheat roots of *Pantoea* sp. YR343 with mcherry fluorescence. C. GFP *Pantoea* sp. YR343 colonies from a pellicle. 40
Figure 3.9. Figure 4.22. Using ImageJ to calculate number of cells in each symplasmata. ImageJ can separate the fluorescent cells and watershed to account for error. The new image (right) can be used to count the individual cells. ……...……..40
Figure 3.10. Using ImageJ to calculate number of cells in each symplasmata in WT Pantoea sp. YR343……41
Figure 3.11. Using ImageJ to calculate number of cells in each symplasmata as a percentage of symplasmata vs. total cells in WT Pantoea sp. YR343…….41

Figure 3.12. WT and transposon mutant symplasmata formation of *Pantoea eucalypti* 299R. *LrhA:*Tn5 does not form symplasmata.[4] 42
Figure 3.13. *LrhA:*Tn5 does not form symplasmata in a pellicle. 42
Figure 3.14. *RcsA:*Tn5 clusters with no capsule in a pellicle. 42
Figure 3.15. Depiction of transposon insertion into the gene encoding DNA helicase using BLAST. 43
Figure 3.16. Location of PMI39_00093 using IMG with descriptions of adjacent genes. 43
Figure 3.17. Similar pellicle formation for WT (left) and BB4 (right). 44
Figure 3.18. Trypan blue phenotype for BB4 (right) compared to WT (left). 44
Figure 3.19. Significant biofilm defect for BB4 compared to WT *Pantoea* sp. YR343 in a crystal violet biofilm assay. 44
Figure 3.20. Degradation of c-di-GMP by a diguanylate phosphodiesterase. 45
Figure 3.21. Equal growth of transposon mutants compared to WT. 46
Figure 3.22. Equal biofilm development of transposon mutants compared to WT. 46
Figure 3.23. Swimming motility for WT (left), G11 (center), and G7 (right). 47
Figure 3.24. Pellicle defect for G11 (right) compared to WT (left). 47
Figure 3.25. Growth in a 96-well plate. Little to no growth for salicin to salicin cultures and delayed growth for glucose to salicin cultures. 49
Figure 3.26. R2A cultures showing no growth. 49
Figure 3.27. Growth in 250 mL of MOPS. Delayed and slightly reduced growth for salicin to salicin cultures and delayed growth for glucose to salicin cultures. 50
Figure 3.28. Growth in 250 mL of MOPS with glucose or salicin compared to cultures grown in R2A. MOPS + glucose grows similarly to R2A, but MOPS + salicin has delayed growth of about 12 hrs. 50
Figure 3.29. Comparing Glycoside hydrolase family 1 genes. Aligned using TCoffee, formatted into a Newick file using Clustal W2, and viewed and edited using Dendroscope. 51
Figure 3.30. Growth curve of transport mutants grown in R2A media. 55
Figure 3.31. Pellicles different from the WT's (right). F11 (left), F12 (second from left), and BB11 (second from right). 55
Figure A.1. Modified pk18mobsacB plasmid (left). Transformation of the plasmid with no insertion (top right) and with insertion (bottom left). 64

Figure A.2. Gel electrophoresis showing presence of *rcsA* insert into pk18mobsacB plasmid.... 65
Figure A.3. Diagram of screen for *rcsA* clean deletion mutant..... 65

AHL: N-acyl homoserine lactone
C-di-GMP: Bis-(3ÅL-5ÅL)-cyclic dimeric guanosine monophosphate
EPS: exopolysaccharide
IAA: Indole Acetic Acid
LrhA: LysR homolog A; regulator of flagella
LuxR: luminous emittance regulator; master regulator of bioluminescence in *Vibrio fischeri* (EsaR and SdiA are homologs)

PGPR: Plant-growth promoting rhizobacteria

pSRK*:rcsA*: IPTG-inducible overexpression of *rcsA*
QS: Quorum sensing
RcsA: Regulator of Capsular Synthesis
***rcsA*:Tn5**: transposon mutant of *rcsA*
UDP: UDP-phosphate galactose phosphotransferase

CHAPTER ONE: BACKGROUND

Complex Communities

The rhizosphere encompasses a complex and diverse community composed of a host plant and its associated community. This community includes many organisms, such as nematodes, fungi, and bacteria. Its composition is influenced by both biotic and abiotic factors, such as temperature, pH, and moisture.[9, 10] Compared to bulk soil, the rhizosphere is a nutrient-rich environment containing sugars, amino acids, organic acids, carbon, and other small molecules from root exudates.[11]

Host plant species and plant richness can greatly alter microbial interactions. This results in the coevolution of plants and the soil community. The establishment of early land plants was facilitated by their interaction with symbiotic fungal associations. Molecular interactions with epiphytic, symbiotic, and pathogenic microbes have shaped the evolution of land plants overtime.[12, 13]

The various interactions between plants and its associated community can alter the community as a whole. In addition, the community and environment of the plant host is a vital determinant of the community structure. Plants, fungi, and microbes are also all affected by spatial scales, plant richness, species identity, and overall community characteristics.[14] The many conditional variables affecting complex communities in the rhizosphere require it to be meticulously studied to elucidate the factors contributing to plant health and fitness.

Plant-Microbe Communities

There are tens of thousands of species of microbes associated with plant roots and some can be crucial for plant health. Plants affect the microbiome through the exudation of compounds. At the same time, microbes provide resources, modulate hormone levels, and compete for nutrients and space.[11, 15] Depending on the host and microbe species and environmental conditions, microbes in the rhizosphere have the opportunity to be harmful, neutral, or beneficial to the plant.[11]

There are reciprocal impacts on plants and microbes. Plants influence the rhizosphere by releasing organic acids, sugars, amino acids, fatty acids, vitamins, growth factors, hormones, and antimicrobial compounds.[16-18] How the microbial community structure is organized, however, is not well-understood. Bakker et. al. shows no consistency for operational taxonomic units (OTUs) between different host species. The microbes depend on biotic and abiotic characteristics, like carbon and soil moisture, which are affected by plants.[14,19]

Plant-growth promoting rhizobacteria (PGPR) can reduce the incidence of soil borne diseases. PGPR can limit pathogen success by consuming nutrients, stimulating the plant immune system, and/or producing biostatic compounds.[15, 20, 21] Rhizobacteria can act as biocontrol agents. They can locally antagonize pathogens or cause systemic resistance of the entire plant with the use of siderophores and antibiotics. This biocontrol could improve crop systems.[15, 22, 23]

PGPR can also help in the solubilization of mineral phosphates and other nutrients, stabilize soil aggregates, improve soil structure and organic matter content, and enhance resistance to stress (Figure 1.1).[18, 24] These factors affect the host's growth, development, physiology, and metabolism.[20]

Identifying essential functions, such as biofilm formation and motility, and their expression in bacteria in response to plant signals will define what genes are required for bacterial colonization. This knowledge will allow researchers to create minimal bacterial genomes that demonstrate effective colonization and rhizosphere competence.[4] Overall, manipulating the microbiome can reduce plant disease, increase agricultural production, and reduce chemical use and emissions of greenhouse gasses.

Populus deltoides Microbiome

A major source for biofuel and plant-microbe interaction studies is *Populus deltoides* or the poplar tree. There is a renewed interest in poplars as a major source of bioenergy where their wood is converted into transportation fuel and other energy resources (Figure 1.2). *Populus deltoides* trees are sources of bioenergy by producing cellulose, which is the source for biofuels.[25] Plant-based biofuels provide a renewable resource for gasoline additives ethanol and

butanol. As of now, a major obstacle toward realizing the potential of biofuels is the high cost of production.[26]

Poplars are a model for woody perennials and physiological research because they can be easily utilized as a short-rotation woody crop with their extraordinary growth rates. They can also grow on land not suitable for food, so they do not compete with agriculture. A poplar increases carbon sequestration, which reduces the carbon debt from land use changes. It also has the first fully sequenced tree genome. [25, 27] The poplar can be a dominant keystone species and vital to the pulp and paper industry as well as biofuel production.

Proteobacteria and *Actinobacteria* dominate the microbial community of mature *Populus deltoides* roots.[25] The rhizosphere of the poplar provides carbon and energy sources for microbial communities by exporting organic molecules and nutrients.[25] In addition to the impact of plants and microbes, abiotic factors, like soil type, pH, geography, and season, affect the poplar-microbe interactions. Understanding the complex relationship between *Populus deltoides* and its resident microbes could promote poplar growth and development, increase its resistance to disease, and improve its phytoremediation potential.[28]

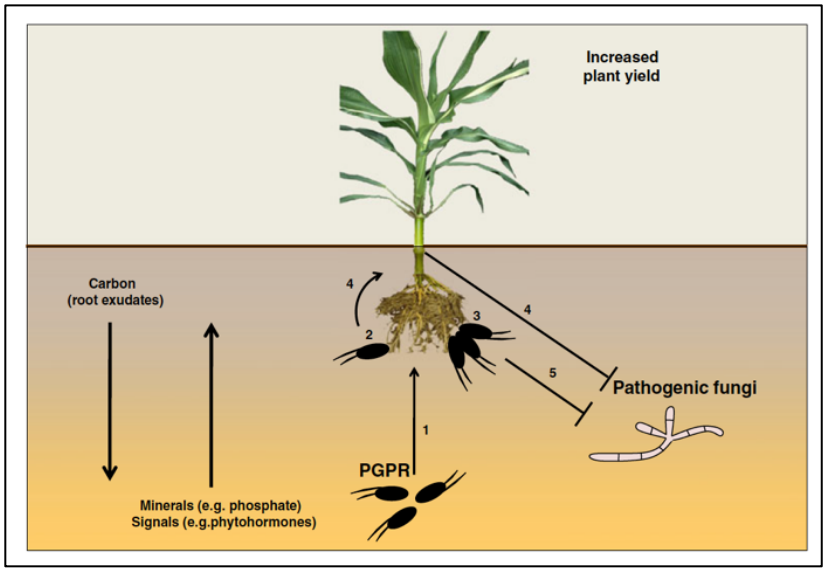


Figure 1.1. Beneficial plant-microbe interactions in the rhizosphere. 1) Motility, 2) Adherence, and 3) Growth are the essential steps to compete in the rhizosphere. PGPR strains can release nutrients and phytohormones as well as inhibit root diseases caused by pathogens by 4) causing the plant to elicit Induced Systemic Resistance (ISR) or 5) directly producing secondary metabolites.[4]



Figure 1.2. Hybrid poplars planted as row crops. Can be processed into ethanol as alternative fuel.[2]

Pantoea sp. YR343

Pantoea is from the *Enterobacteriaceae* family and has been isolated from plants, humans, and the natural environment. Some members of the genus *Pantoea* are infamously pathogenic. *Pantoea stewartii* is known for Stewart's Wilt Disease, which causes corn crops to wilt. *Pantoea agglomerans* causes crown and root gall disease and gysophila and beet plants. Also, *Pantoea ananatis* causes bacterial blight and dieback of *Eucalyptus*, stem necrosis of rice, and brown stock rot of maize.[29, 30] *Pantoea* has a broad host range and pathogenic potential.[31]

However, some *Pantoea* strains have been shown to be beneficial to plant hosts. *Pantoea* sp. YR343 is not pathogenic when applied to the leaves or roots of selected plant hosts and readily colonizes plant roots (Figure 1.3). *Pantoea* sp. YR343 is a motile and rod-shaped bacterium isolated from the roots of *Populus deltoides.*[1] The gamma-proteobacterium *Pantoea* sp. YR343 is one of the more vigorous colonizers of *Populus deltoides* and could provide greater benefits to poplar trees with increased colonization. Some characteristics that promote its ability to survive in the rhizosphere and associate with its plant hosts are swimming and swarming motility, its ability to solubilize phosphate, and its production of IAA. The motility is key because it can avoid hostile conditions and locate and form colonies on the roots in the soil.[1, 32]

Pantoea sp. YR343 could be a beneficial colonizer because it possesses the ability to solubilize phosphate as well as produce the phytohormone indole-3-acetic acid (IAA).[1] The phosphorous amount in the soil is high but mostly insoluble. A microbe's ability to solubilize phosphate could be essential for plant growth. The production of IAA has the ability to affect plant cell division, extension, differentiation, stimulate germination, increase xylem and root development, control vegetative growth and root formation, and mediate responses to environmental stresses.[29]

Colonization and Biofilm Formation of Microbes

Bacteria need to be able to establish themselves in the rhizosphere at a sufficient population density to have a beneficial effect. To accomplish this, the plant-microbe field needs a greater understanding of how bacteria efficiently colonize the root system and become fierce competitors against other microorganisms.[23]

A major factor in colonization is quorum sensing, a signaling mechanism in bacteria that regulates biofilm formation, motility, and other morphological and cellular processes. N-acyl homoserine lactone (AHL) signal molecules accumulate in environments of a sufficiently dense population or a quorum. This quorum of signal-generating bacteria coordinates to express specific target genes. Quorum sensing is most often regulated by LuxR. This system regulates functions required for host-microbe interactions, which makes it significant for promoting beneficial microbial activities (Figure 1.4).[33]

A general quorum sensing mechanism involves LuxI-dependent production of AHL signaling molecules that freely diffuse across biological membranes. The *luxR* gene encodes for a signal receptor that is an acyl-HSL-responsive transcriptional activator that resides in the cytoplasm. Upon binding of the AHL molecule, LuxR binds to its recognition site and interacts with RNA polymerase to stimulate transcription of a wide variety of genes depending on the bacterial strain. In *Vibrio fischeri*, this results in transcription of the luminescence operon and the production of light (Figure 1.5).[6, 34, 35]

Bacteria live as independent planktonic cells or members of organized surface-attached communities called biofilms. The cells transfer from motile to sessile and attach to a surface to form a biofilm. Motility is key for the initial interaction and movement along the surface.[36, 37]

Biofilms are formed in response to environmental conditions and cues[38] and can protect a microbial community from stresses, immune responses, and antibacterial agents. Within a biofilm, there are gradients of nutrients, waste products, and signaling factors that produce a heterogeneous environment. [7, 39-41] Cells within a biofilm can experience different local environmental conditions which can influence gene regulation and lead to functional diversity within the community. The molecular mechanisms that drive biofilm formation have been the subject of much research.[42]

Recent research has shown that the secondary messenger c-di-GMP plays a significant role in driving biofilm formation. The synthesis of c-di-GMP is driven by diguanylate cyclases (DGCs), whereas the degradation of c-di-GMP is driven by phosphodiesterases (PDEs).[7, 43] C-di-GMP signaling cascades begin with the activation of a DGC or repression of a PDE followed by binding to an effector component, which produces a molecular output.[44] Generally, bacteria form biofilms at high c-di-GMP cellular levels and disperse at low c-di-GMP levels. The specific mechanisms behind this observation have proven to be a "regulatory nightmare" due to numerous c-di-GMP signaling systems, questions of specificity, and the diverse intracellular and environmental stimuli that serve specific targets.[45,46] The action of DGCs and PDEs is well-characterized, but research on specific effectors and environmental cues need to be conducted in order to gain a greater understanding of the scope of c-di-GMP signaling cascades.

C-di-GMP is a key player in the switch between motile planktonic and sedentary biofilm-associated bacteria. C-di-GMP binds to a range of effector components and controls diverse targets, like transcription and the activities of enzymes. Generally, it stimulates the biosynthesis of adhesins and exopolysaccharide matrix substances in biofilms and results in a decrease in various forms of motility.[7]

It has also been proven that c-di-GMP affects the transcription of target genes. The secondary messenger binds to structurally and functionally unrelated proteins (like transcription factors) and even to RNAs (riboswitches). Therefore, it can act at the transcriptional, posttranscriptional, and posttranslational levels. For example, the *P. aeruginosa* transcription factor, FleQ, directly binds to c-di-GMP, which antagonizes the activity of c-di-GMP because FleQ activates the expression of flagellar genes and represses the biofilm promoting operon (Figure 1.6).[7]

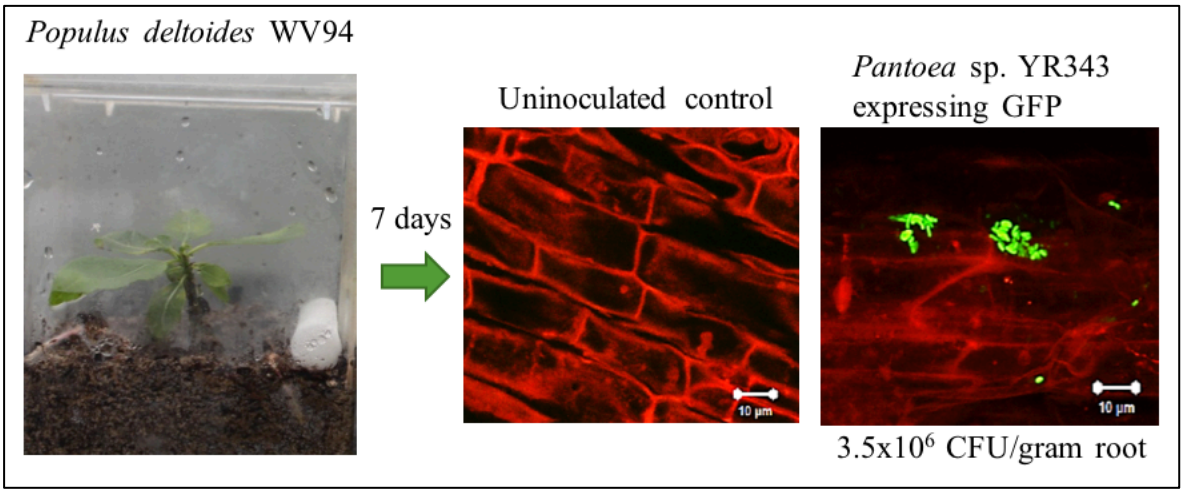


Figure 1.3. *Pantoea* sp. YR343 colonizing *Populus deltoides*. *Populus deltoides* WV94 cuttings grown in presence or absence of *Pantoea* YR343 expressing GFP for seven days. We detected plant roots using red autofluorescence and YR343 using GFP (green fluorescent protein) fluorescence.

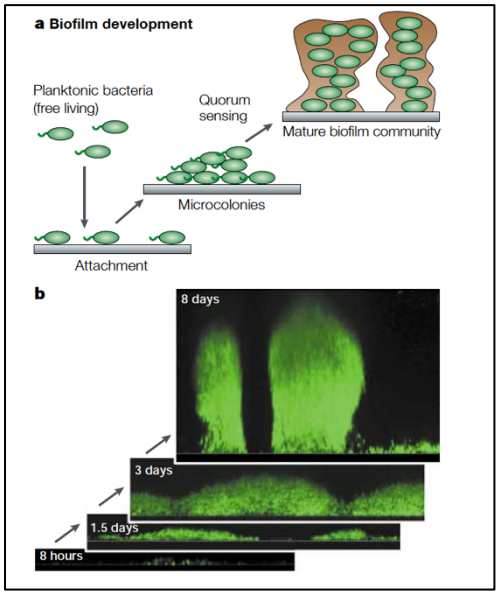


Figure 1.4. Quorum sensing and biofilms. a. Steps involved in biofilm development. b. Confocal microscope images of P. aeruginosa developing a biofilm over time while producing GFP. The tower structures after 8 days are 100 um high.[6]

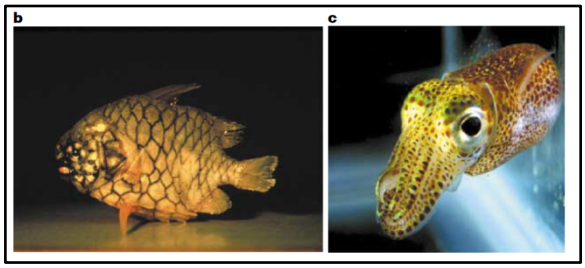


Figure 1.5. Symbiotic bioluminescence as a result of lux-gene organization. b. Australian pinecone fish has a lower light organ on the haw that contants ~10^10 *V. fischeri* cells per ml fluid. Pinecone fish use the light to search for prey at night. c. Hawaiian bobtail squid with an organ with ~10^11 *V. fischeri* cells per ml close to the ink sac. Bobtail squids emit light downward to blend with the moon and starlight to become invisible to predators.[6]

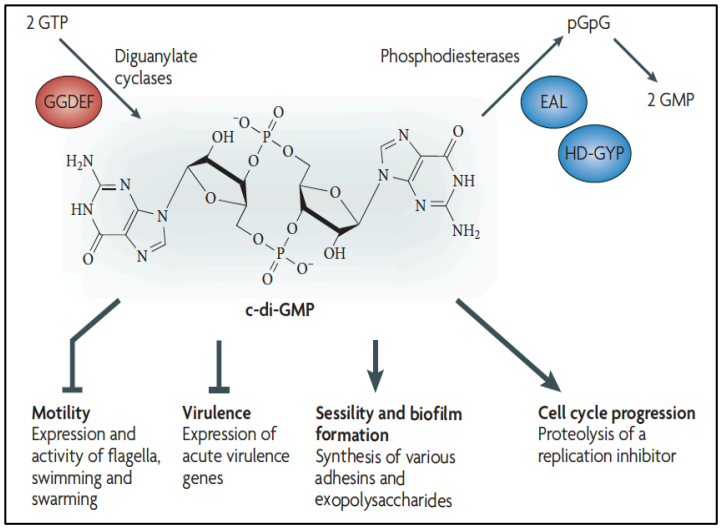


Figure 1.6. Physiological functions and structure of c-di-GMP. c-di-GMP is controlled by diguanylate cyclases that carry GGDEF (red) domains and specific phosphodiesterases that carry EAL or HD-GYP domains (blue). c-di-GMP can reduce motility by downregulating flagellar expression or interfering with flagellar motor function. High c-di-GMP levels stimulate biofilm-associate functions, like the formation of fimbriae and other adhesins and various matrix EPS.[7]

Exopolysaccharide Production

Exopolysaccharides (EPS) can provide survival advantages by preventing predation, impeding desiccation, and acting as an adhesive for microbes. EPS are layers of carbohydrates external of the cell wall. They are not water soluble.[47] The production of EPS is a widespread characteristic of gram-negative bacteria.[48]

EPS production is often correlated with virulence.[49] EPS capsules protect pathogens against recognition by plant defenses, bind water to keep bacteria moist, and retain nutrients and ions released from the plant. The capsules are favorable for bacterial multiplication, aid in the spread of bacteria, but can act as virulent factors.[48]

While EPS production is harmful from a pathogenic strain like *P. stewartii,* EPS in a non-pathogenic and even PGPR strain can protect plant roots from various stresses.[50] EPS can enhance water retention in the microbial environment as well as regulate the diffusion of carbon sources, like glucose. Studies on the EPS-producing bacterium, *Panotea agglomerans NAS206*, showed a positive effect on plant growth by affecting rhizosphere soil aggregation and

macroporosity.[51] Mutants affected in EPS biosynthesis were hindered in their capacity to initiate wheat root colonization at the root hair zones compared to the wild-type.[52] Efficient EPS production could potentially contribute to a more competitive strain and provide greater benefits to plants.

A study by Bernhard et al. compared the gene cluster for EPS synthesis in *P. stewartii* and *P. amylovora.*[48] They determined that the *P. amylovora* gene cluster, *ams*, is 7 kb and equivalent to *P. stewartii's* cps gene cluster.[48] In a later study, they measured the glucose-galactose ratios of the capsules and determine their structures. They determined that they have similar structures with glucose, galactose, and glucornic acid as the main components. The operons had similar organizations and homology. There were slight differences in structure, which indicates that ams and cps gene clusters adapted to different host plants.[48, 53,54]

RcsA: Regulator of Capsule Production

RcsA is a DNA binding protein related to response regulators RcsB, C, and D. However, RcsA is not regulated by phosphorylation. RcsA binds with RcsB to activate transcription of genes (Figure 1.7). These proteins are likely involved in capsular polysaccharide production. RcsA has also been shown to repress genes for flagella synthesis. RcsA can be degraded by the Lon protease and negatively regulated by a heat-stable nucleoid-structuring protein (HNS).[8]

RcsAB transcriptionally activates EPS biosynthesis in *P. stewartii.*[48] EsaR, a LuxR homolog, represses transcription of *rcsA* by binding in the promoter region. Otherwise, RcsA binds with RcsB to form a heterodimer complex that activates the expression of *rcsA*. RcsAB also activates the cps gene cluster.[55, 56] RcsA stabilizes RcsB-DNA complexes.[57] Wehland et al. identified the RcsAB box as TaAGaatatTCctA.[58]

Overall, cell interaction with surfaces activates the Rcs regulon, which plays a role in development of biofilms on surfaces.[8] RcsA, B, C, D, and F are all predicted to be in *Pantoea* sp. YR343.

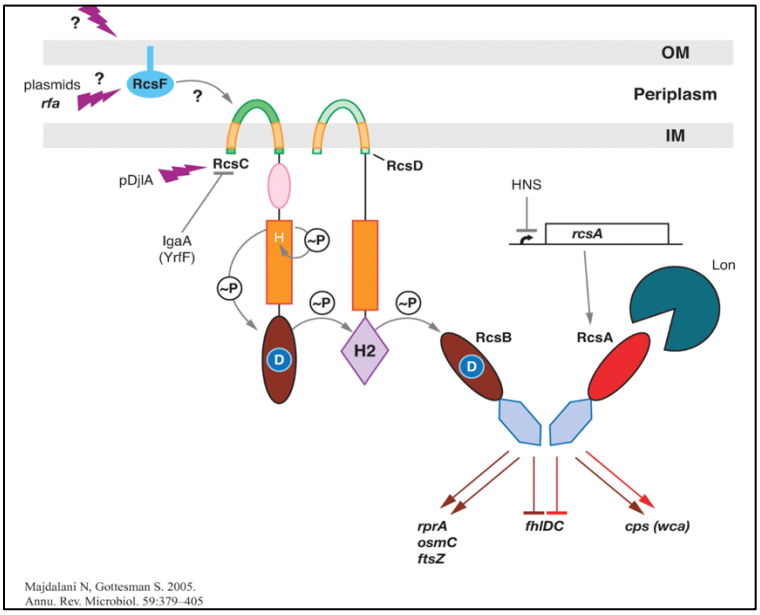


Figure 1.7. Signal transduction pathway for RcsA, B, C, and D genes. Phosphate transfer from RcsC to RcsB is shown. HNS negatively regulates *rcsA* transcription.[8]

Regulation of *RcsA* in *Pantoea stewartii*

Some of the first members of the genus *Pantoea* were recognized as plant pathogens. Since then, *Pantoea* strains have been constantly isolated from aquatic and terrestrial environments. In *Pantoea stewartii*, quorum sensing affects adhesion, motility, dispersion, and EPS production. As a result, quorum sensing plays a major role in the development of Stewart's wilt disease in corn.[55]

Ramchandran et al., 2014, have analyzed LrhA and RcsA in *P.* stewartii in a quorum sensing context. A density-dependent quorum-sensing (QS) system temporally controls the production of the EPS stewartan in *P. stewartii* and regulates RcsA and LrhA. The QS system is regulated by a transcription factor, EsaR, which belongs to the LuxR family. P. *stewartii* contains two LuxR homologues: EsaR and SdiA. The LuxI homolog, EsaI, synthesizes the cognate acylated homoserine lactone (AHL). EsaR recognizes the AHL signal, N-3-oxo-hexanolyl-homoserine lactone, which enables EsaR to sense changes in cell density. EsaR binds to specific 20-bp regulatory sequences in promoter regions called esa boxes when AHL is at a low density. Once it binds to an esa box, it can repress or activate transcription of downstream genes. At high cell

density, AHL binds to EsaR, which disables it from binding to DNA. This leads to derepression or deactivation of gene expression.[59, 60] This gene expression could affect a variety of physiological outputs as a result of QS, like biofilm formation, virulence factor expression or exoenzyme production.

Based on previous and current results, Burke et al. developed an overall QS regulation model for *Pantoea stewartii.* Previous studies showed that EsaR is capable of self-inactivation. EsaR regulates both *rcsA* and *lrhA*. It represses *rcsA*, while it activates *lrhA*. RcsA regulates genes involved in capsule production. In Burke et al.'s study, they determine that LrhA also represses RcsA as well as genes involved in surface motility and adhesion (Figure 1.8).[3]

Function of *RcsA* in *Pantoea stewartii*

A paper describing the roles of RcsA and LrhA in *P. stewartii* was recently published, and the phenotypes described are consistent with the phenotypes observed for our mutants (described below). In *P. stewartii*, quorum sensing affects adhesion, motility, dispersion, and EPS production. As a result, quorum sensing plays a major role in the development of Stewart's wilt disease in corn. Burke et al. studied the functions and virulence effects of transcription factors, LrhA and RcsA, in *P. stewartii.* Their transcriptome analysis showed that RcsA primarily regulated genes encoding proteins involved in capsule production and LrhA regulated genes encoding hypothetical proteins. They validated their transcriptome analysis with qRT-PCR, which also confirmed a three-fold repression of *rcsA* by LrhA. They performed phenotypic analyses on the *lrhA* and *rcsA* knockouts. The main results of these analyses showed that the *rcsA*-knockout had a significant reduction in capsule production as compared to the wild-type. The *lrhA*-knockout showed a significant reduction in surface area covered in a swarming motility assay as compared to the wild-type (Figure 1.9).[3]

While *Pantoea* sp. YR343 and *P. stewartii* are from the *Pantoea* genus and code for the transcription factors, LrhA and RcsA, it is unknown whether LrhA and RcsA regulate the same genes. Notably, *Pantoea stewartii* is pathogenic and causes Stewart's wilt disease, whereas *Pantoea* sp. YR343 appears to be non-pathogenic on all tested plant hosts (poplar, Arabidopsis, wheat). In addition, *Pantoea* sp. YR343 only has one LuxR homolog, which is unlike *P. stewartii* with two. The *Pantoea* sp. YR343 LuxR homolog is more similar to *Pantoea stewartii's* SdiA

LuxR homolog (66% amino acid identity) than EsaR (26% amino acid identity). Therefore, it is likely that the transcription factors are regulated differently in *Pantoea* sp. YR343 than *P. stewartii.* While *P. stewartii* is different from *Pantoea* sp. YR343, the P. *stewartii* research helps in forming expectations for this study. We formed a phylogenetic tree for *Pantoea* sp. YR343 with other closely related species in Figure 1.10 below.

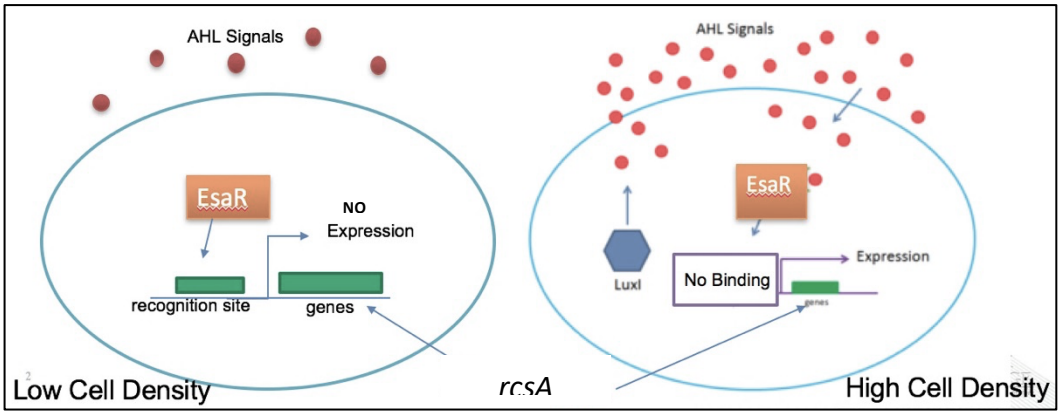


Figure 1.8. Regulation of *lrhA* and *rcsA* in *Pantoea stewartii*. At high cell densities, EsaR forms a complex with AHL and becomes inactivated. It cannot bind to the DNA or coordinate the expression of genes. At low cell densities, EsaR is free to bind to its recognition site and coordinate the expression of genes, like *lrhA* and *rcsA*.

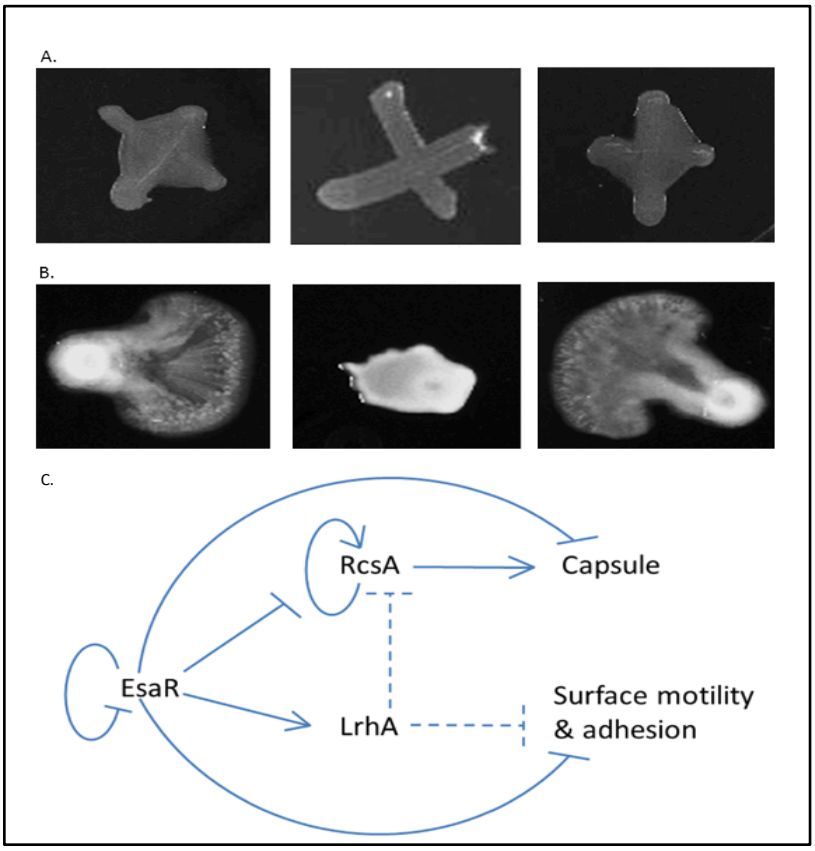


Figure 1.9. RcsA and Lrha in *Pantoea stewartii*. A. Capsule assay showing reduced capsule in RcsA knock-out mutant (center) compared to WT (left). Recovered capsule in complementation (right). B. Swarming assay showing reduced swarming in LrhA knock-out (center) compared to WT (left) and complementation (right). C. Regulatory model of RcsA and LrhA.[3]

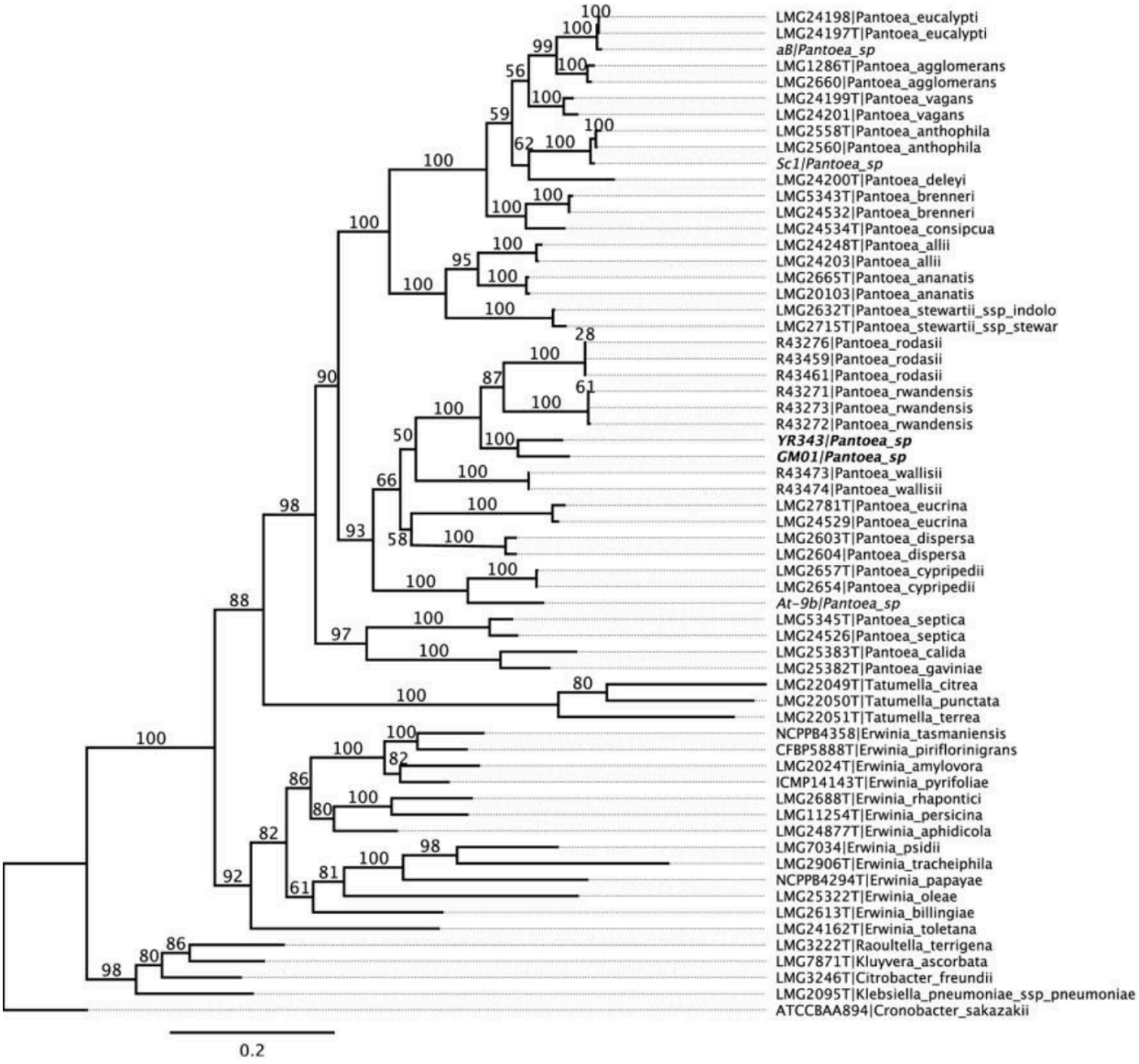


Figure 1.10. Phylogenetic tree of *Pantoea* YR343 with other *Enterobacteriaceae* species.[1]

CHAPTER TWO: The Function and Regulon of Transcription Factor RcsA in *Pantoea* sp. YR343

Selecting RcsA

We isolated the *rcsA* transposon mutants from a transposon library previously created in our lab during a screen for mutants that failed to respond to high levels of Bis-(3ÅL-5ÅL)-cyclic dimeric guanosine monophosphate (c-di-GMP), which is a soluble molecule that acts as a second messenger in bacteria. High levels of c-di-GMP are generally associated with increased EPS production, biofilm formation, and reduced motility. For this screen, the assumption was made that root colonization was equivalent to biofilm formation because biofilm formation is key to colonization and that mutants defective in their response to high c-di-GMP levels may have defects in root colonization. The screen was conducted by overexpressing a diguanylate cyclase, which is an enzyme that produces c-di-GMP, in a transposon library background. WT cells overexpressing this diguanylate cyclase produce a characteristic wrinkly colony that binds Congo Red (Figure 2.1). Transposon mutants that displayed different colony phenotypes on Congo Red plates were selected as candidate mutants defective in their response to high levels of c-di-GMP and potentially defective in biofilm formation/root colonization.

The insertion sites of three of the transposons mapped to a gene with predicted homology to *rcsA* (PMI29_02189, 92% amino acid identity to *P. stewartii's rcsA*). The predicted sequence of RcsA includes a C-terminal DNA binding domain with a helix-turn-helix motif. The transposon insertion sites mapped to base pairs 17 (mutant DD5), 18 (mutant G4), and -3 (mutant AA4) of the predicted *rcsA* sequence. Based on the transposon insertions near the 5' end of the gene, it is likely that these mutants represent loss of RcsA function (Figure 2.2). Due to the observed phenotypic similarities between the three transposon mutants, transposon mutant G4 was primarily used for detailed characterization studies.

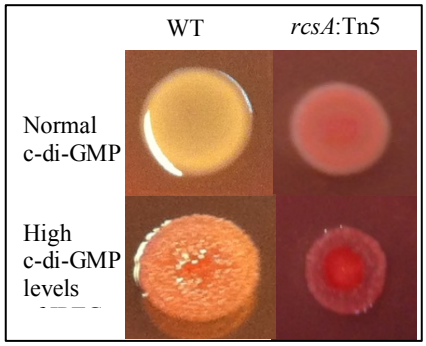


Figure 2.1. WT and *rcsA:*Tn5 on Congo Red plates (top) v. overexpressing c-di-GMP with induction of IPTG on Congo Red plates (bottom).

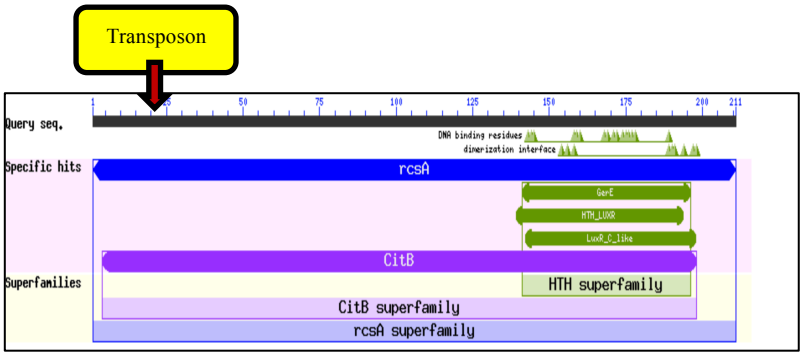


Figure 2.2. RcsA sequence with known domains created by BLASTp. Transposon enters at base pair 18.

Capsule Production. Wild-type and *rcsA*:Tn5 strains were grown overnight in Luria's broth (LB) at 28°C with shaking. Fresh LB was used to adjust the cultures to an OD_{600} of 0.05 and the cultures were grown again at 28°C to an OD_{600} of 0.2. The strains were then cross streaked on CPG agar plates (0.1% casamino acids, 1% peptone, 1% glucose (CPG), and 1.5% agar) to observe capsule production.[3]

Pellicles. Pellicles were grown by adding 5 µL of an overnight culture to 5 mL SOBG[61] in 5 mL glass tubes at 28°C for 72 hours without shaking.

Crystal violet biofilm assay. Biofilm assays were conducted using the protocol described by O'Toole and Kolter, 1998, with a few modifications.[62] An overnight culture was diluted 1:100 into LB and grown statically in a 96-well plate covered in breathable tape (Breathe-EASIER, Diversified Biotech) at 28°C for 72 hours. Adherent cells were stained with 0.1% crystal violet. The crystal violet stains on the biofilms were dissolved using a modified solution containing 10% SDS dissolved in 80% ethanol. Finally, absorbance was measured at 550 nm using a BioTek Synergy 2 microplate reader and normalized according to OD_{600}.[1]

Wheat root colonization. Wheat seedlings were surface-sterilized by washing in a bleach solution containing 0.01% Tween-20, rinsed, washed in 70% ethanol, and rinsed again as described in Bible et al., 2016.[1] Our lab has developed a protocol to inoculate wheat seedlings with *Pantoea* sp. YR343 based on Amellal et al.'s methods (1998).[51] Briefly, we added 15 mL of total culture (OD_{600} of 0.01) to 100 mL of Fahreus media and placed two seedlings in each container. The seedlings grew for one week with ample sunlight. After this period, they were imaged on the confocal laser microscope for qualitative assessment and harvested by rinsing excess media, grinding with glass beads, and plating on new plates. The new plates were quantified for cell count. There were four to five plant replicates for each sample collected in two to three separate rounds of colonization.

Monosaccharide analysis. To wash the cells before isolating the EPS, we grew cells overnight at 28°C with shaking in 5 mL of LB. We then inoculated 25 µL overnight culture to 250 mL of SOBG and grew at 28°C for 72 hours. We collected the cells via centrifugation and washed in PBS before incubating with shaking at 30 °C for 1.5 hours and repeating. We collected the cells again and treated them with proteinase K to a final concentration of 200 ug/mL. To isolate the EPS after incubating ON at 37 °C, we extracted the supernatant using phenol-chloroform and

precipated the sugars with 95% ethanol in the freezer. We washed the pellets with 70% ethanol, resuspended them in water, and dialyzed them with a Slide-a-lyzer dialysis cassette overnight. We redialyzed the samples for one hour before collection. The glycosyl composition analysis was performed by the Complex Carbohydrate Research Center (University of Georgia).

RNA extraction, sequencing, and analysis. We extracted RNA from 3 WT and 3 mutant ON cultures in R2A media and 3 WT and 3 mutant pellicles grown in SOBG with a Qiagen RNeasy RNA extraction kit. The samples were sequenced by GENEWIZ Next Generation Sequencing Services. We performed a transcriptome analysis using the KBase workflow to create an RNA sample set, align and assemble the reads, and identify the predicted genes and their functions that are differentially expressed among the samples.

Promoter constructs. We developed the promoter constructs using a pPROBE:GFP vector. We PCR amplified the promoter region for each gene, digested the vector and PCR fragment, and ligated them together. We then transformed them into *E. coli* TOP10 cells and electroporated the extracted plasmid into *Pantoea* sp. YR343.

Overexpression constructs. We overexpressed *rcsA* as described in Khan et al., 2008. Briefly, we cloned the strains into the replicating, IPTG-inducible vector pSRK. Expression is induced by the addition of 2 mM IPTG.[63]

Results

rcsA:Tn5 has an EPS Production Defect

Since the *rcsA:*Tn5 mutants were isolated in a screen to identify mutants that failed to respond to high c-di-GMP levels, we wanted to examine their phenotypes under normal growth conditions. To do this, we cured the *rcsA:*Tn5 mutants of the plasmid encoding a constitutively expressed diguanylate cyclase using repeated rounds of growth and plating with antibiotic selection. The cured strains were then compared to control strains to examine the effect of RcsA loss of function on biofilm formation and EPS production.

Congo Red plates and capsule production assays were used to examine phenotypic differences in EPS production and/or composition. These results show that the cured *rcsA:*Tn5 mutant shows stronger Congo Red binding than the WT strain (Figure 2.3). There were also differences between *rcsA:*Tn5 and the WT with regard to capsule production. Indeed, the

*rcsA:*Tn5 mutant failed to produce a detectable capsule in this assay. To examine the effect of RcsA overproduction, we constructed a plasmid in which RcsA is expressed from an IPTG-inducible promoter (pSRK-*rcsA*).[63] Overexpression of RcsA in a WT background did not result in any significant changes to Congo Red binding or capsule production, but rather resembled the WT strain (Figure 2.3). Finally, we examined whether high levels of c-di-GMP could overcome the capsule defect in *rcsA:*Tn5. The results of this experiment indicate that the *rcsA:*Tn5 mutant still failed to produce capsule even under high c-di-GMP conditions that promote capsule production in WT (Figure 2.3).

We next wanted to determine whether the EPS composition was different between the *rcsA:*Tn5 and WT strains. To test this, we isolated the EPS from both strains and sent them to the Complex Carbohydrate Research Center for monosaccharide analysis. The results of this analysis showed that the EPS from WT cells is composed primarily of galactose, glucose, glucuronic acid, and mannose (Figure 2.4). The EPS from the *rcsA*:Tn5 mutant, on the other hand, showed reductions in the levels of galactose, glucose, and glucuronic acid (Figure 2.4). This result is particularly interesting since the repeat unit of *P. stewartii* stewartan EPS, the production of which is regulated by RcsA, is comprised of galactose, glucose, and glucuronic acid.[64] These data suggest the possibility that RcsA regulates the production of a similar EPS in *Pantoea* sp. YR343.

To test this possibility, we examined *Pantoea* sp. YR343 for the presence of genes encoding proteins homologous to those involved in stewartan production in *P. stewartii.* Stewartan is synthesized by a suite of enzymes that are encoded by genes organized within an operon.[48, 65] Indeed, we found a gene cluster in *Pantoea* sp. YR343 (PMI39_01835-1848) that is predicted to encode proteins homologous to those involved in stewartan production (Figure 2.5). One of the genes in this cluster (PMI39_1848) encodes a protein that is homologous to *P. stewartii's* undecaprenyl-phosphate UDP-galactose phosphotransferase (*wceG2*). Interestingly, we had also identified a transposon mutant that inserts into the gene PMI39_01848 (abbreviated *UDP:*Tn5) in the same genetic screen that produced the *rscA*:Tn5 mutants. Thus, we also examined the monosaccharide composition of *UDP:*Tn5 and found a similar reduction in glucuronic acid (GlcA), galactose (Gal), and glucose (Glc) compared than the WT (Figure 2.4). This suggests the possibility that the EPS defect found in *rscA*:Tn5 might be due, at least in part, to mis-regulation of the EPS gene cluster PMI39_01835-PMI39_01848.

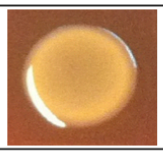
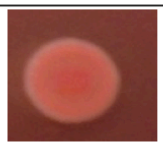
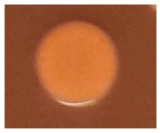
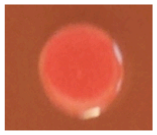
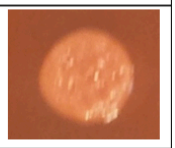
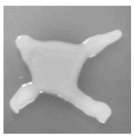
Strain	**WT**	***rcsA*:Tn5**	**pSRK-*rcsA***	***rcsA*:Tn5 with induced c-di-GMP**	**WT with induced c-di-GMP**
A. Congo Red					
B. Capsule					

Figure 2.3. A. Congo Red phenotypes of spotted strains on LB with Congo Red. dye B. Capsule Analysis of cross-streaked strains on capsule media. Assays show EPS effects.

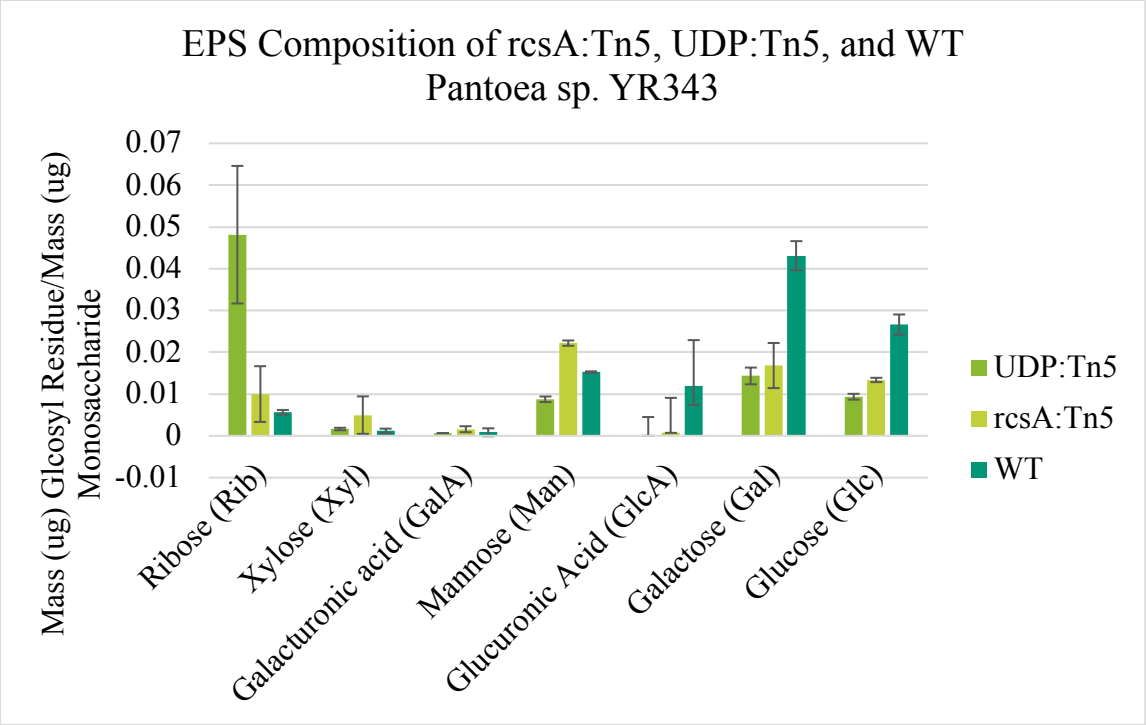


Figure 2.4. Monosaccharide analysis of *rcsA:*Tn5 and *UDP:*Tn5 compared to WT. Error bars show standard deviation. There are two replicates per strain. The bars represent the mean of the replicates.

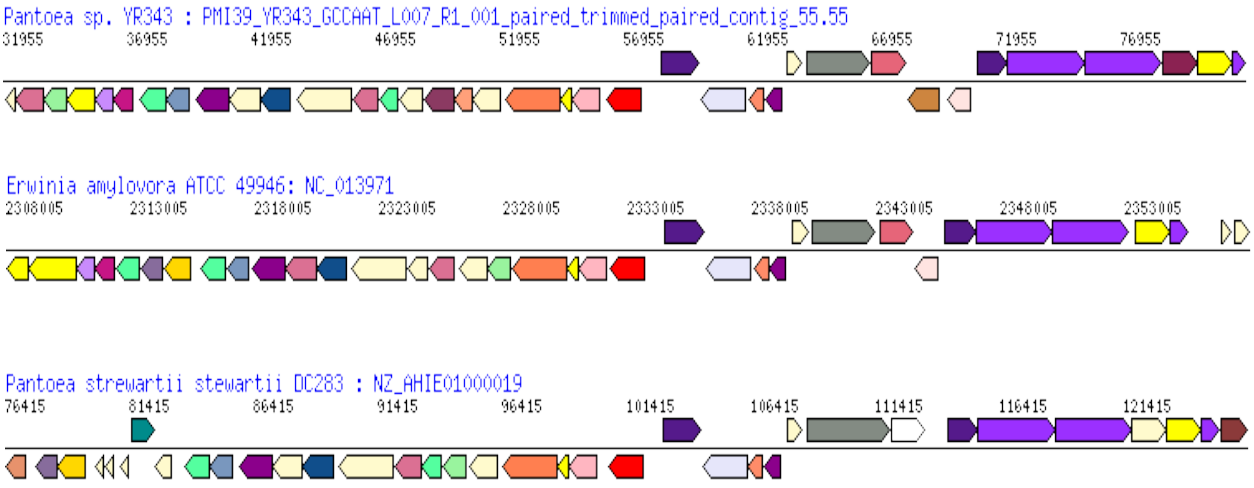


Figure 2.5. Gene neighborhood of *UDP* in *Pantoea* sp. YR343, *Erwinia amylovora,* and *Pantoea stewartii.*

rcsA:TN5 has a Biofilm Formation Defect

We next wanted to determine the consequences of differences in EPS composition by examining biofilm and pellicle formation. Unlike the WT, *rcsA*:Tn5 forms little to no pellicle (Figure 2.6). This pellicle defect could be partially rescued with the induction of c-di-GMP in the *rcsA:*Tn5 background but the pellicle was less structured, suggesting that the EPS composition and/or abundance still differed from WT (Figure 2.6). As before, overexpression of RscA resulted in pellicles that closely resembled those of WT.

We also conducted a crystal violet biofilm assay to analyze biofilm formation for all three of the *rcsA:*Tn5 transposon mutants (AA4, DD5, and G4). In this assay, all of the rcsA:Tn5 mutants showed a significant reduction in biofilm formation compared to the WT (Figure 2.7). These results indicate a role for RcsA's promotion of EPS production in the development of biofilms in *Pantoea* sp. YR343.

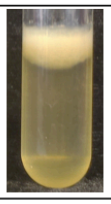
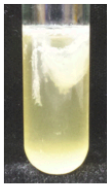
Strain	**WT**	***rcsA*:Tn5**	**pSRK-*rcsA***	***rcsA*:Tn5 with induced c-di-GMP**	**WT with induced c-di-GMP**
Pellicle					

Figure 2.6. Pellicle formation of WT and mutants in *Pantoea* sp. YR343.

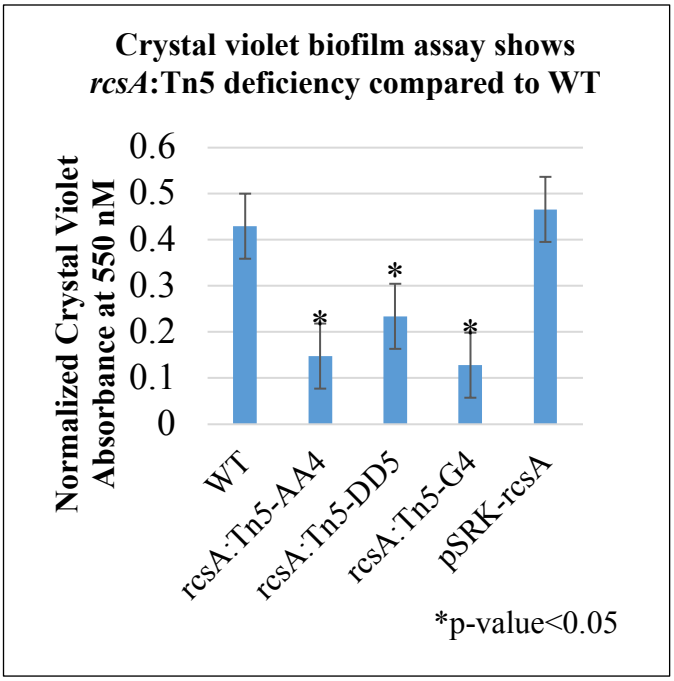


Figure 2.7. Crystal violet biofilm assay shows decreased biofilm formation for *rcsA:*Tn5 mutants compared to WT and pSRK:*rcsA*. Error bars show standard deviation and p-values calculated by T-tests are less than 0.05 where indicated.

rcsA:TN5 has a Colonization Defect

We then wanted to examine if differences in EPS production and biofilm formation found in laboratory assays translated to differences in plant colonization between *rcsA:*Tn5 and the WT strain. In order to monitor colonization of our strains in an actual plant context, we inoculated media surrounding wheat roots with either *rcsA:*Tn5 or WT (Figure 2.8), as well as with co-cultures containing both *rcsA:*Tn5 and WT cells (Figure 2.9). After harvesting, colonization was measured using traditional plating assays (colony counts). Because the transposon carries kanamycin resistance, we differentiated between WT and rcsA:Tn5 by plating on plates containing kanamycin. The results of these studies show that *rcsA*:Tn5 had significantly less colonization than the wild-type in the individual study (Figure 2.8). In the co-culture, however, the levels of colonization of both WT and rcsA:Tn5 were very similar (Figure 2.9). This suggests the possibility that rcsA:Tn5 may colonize more efficiently in the presence of WT due to the formation of mixed biofilms. To test this possiblity, we imaged the localization of WT and *rscA*:Tn5 cells during co-culture with a plant host.

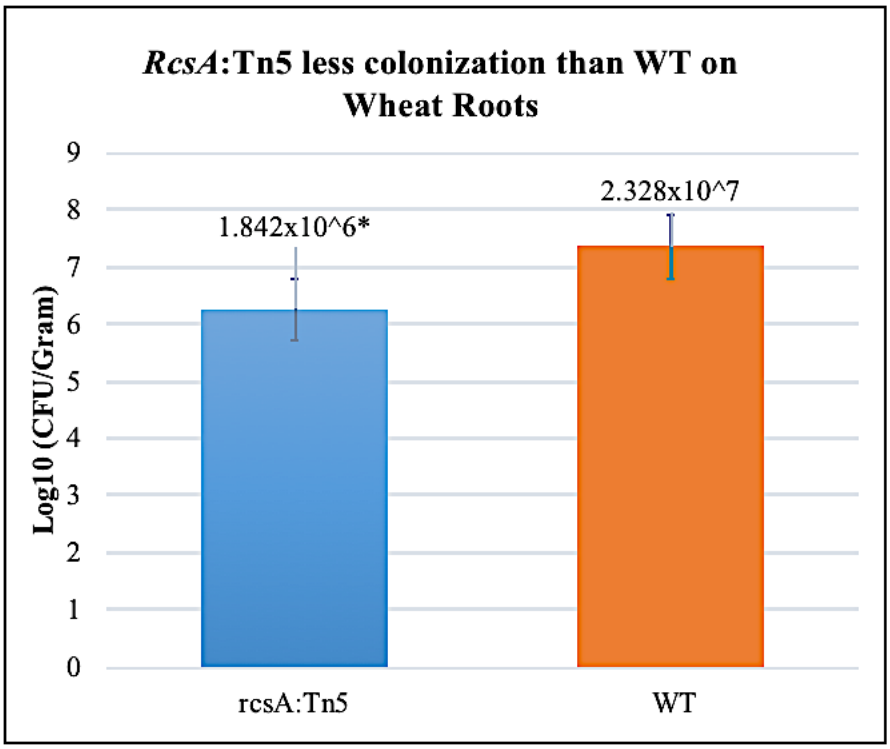


Figure 2.8. Colonization on individual wheat roots. T-test calculated p-value is below 0.05 and error bars show standard deviation. Bars represent the mean of three to four replicates.

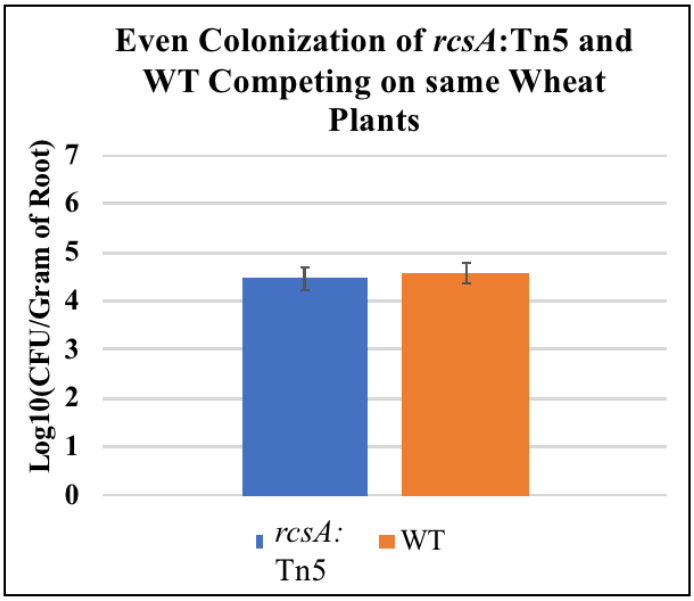


Figure 2.9. Colonization of *rcsA*:Tn5 and WT inoculated on the same wheat roots. Error bars show standard deviation. Bars represent the mean of three to four replicates.

The Expression of *rcsA*

To examine under which growth conditions r*scA* is expressed, we constructed a plasmid in which GFP expression is controlled by the *rcsA* promoter (pPROBE:*rcsA*_promoter). The plasmid was transformed into WT *Pantoea* sp. YR343 and the cells were grown in LB medium. The results indicate that *rcsA* is expressed in an LB culture grown overnight in 28^{o}C based on GFP fluorescence (Figure 2.10). It was also expressed during pellicle formation, biofilm formation, and plant colonization.

The Regulon of RcsA

Previous studies suggest that UDP may be regulated by RcsA.[3, 48] To test this, we constructed a plasmid in which GFP expression is controlled by the *UDP* promoter (pPROBE:*UDP*_promoter) and transformed this construct into both WT and *rscA*:Tn5 cells. Following growth in LB medium overnight, we found that the *UDP* promoter was active in wildtype cells, based on GFP fluorescence (Figure 2.11). Under these same conditions, however, we failed to detect GFP fluorescence in the *rcsA*:Tn5 background (Figure 2.11). These data suggest that UDP expression requires RcsA and is consistent with a role for RcsA in the regulation of UDP. In addition, the RNASeq analysis showed that *UDP* is downregulated in *rcsA:*TN5 compared to the WT, which indicates that RcsA plays a positive role in the expression of *UDP*.

To determine the full complement of genes regulated by RcsA, we next performed a transcriptome analysis. For this analysis, we extracted RNA from WT and *rcsA*:Tn5 cells grown in R2A media or grown under pellicle-forming conditions. To analyze the sequence data, we used the Tuxedo suite through KBase to create an RNASeq sample set, align and assemble the reads, and identify genes that are differentially expressed between *rcsA:*Tn5 and the WT as pellicles and in R2A media as well as differentially expressed genes between the different growth conditions. Tables 2.1 and 2.2 show the differentially regulated genes between *rcsA:*Tn5 and WT in R2A media. There were 746 differentially expressed genes between *rcsA:*Tn5 and WT grown as pellicles. These are displayed as heat maps (Figures 2.12 and 2.13). The most highly represented genes have functions relating to carbohydrate and amino acid transport and metabolism and transcription.

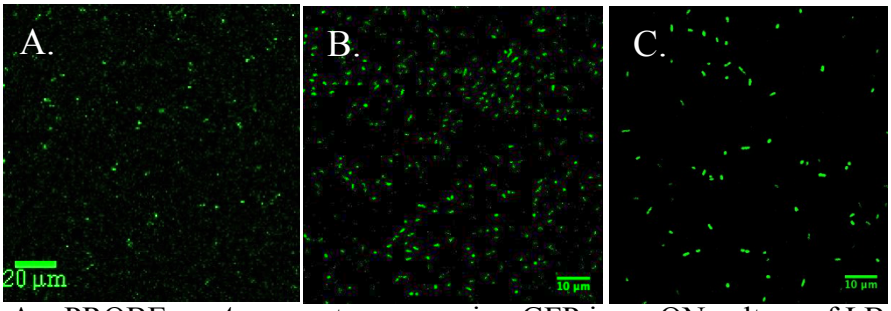


Figure 2.10. A. pPROBE:*rcsA*_promoter expressing GFP in an ON culture of LB. B. Biofilm on a glass slide. C. Pellicle.

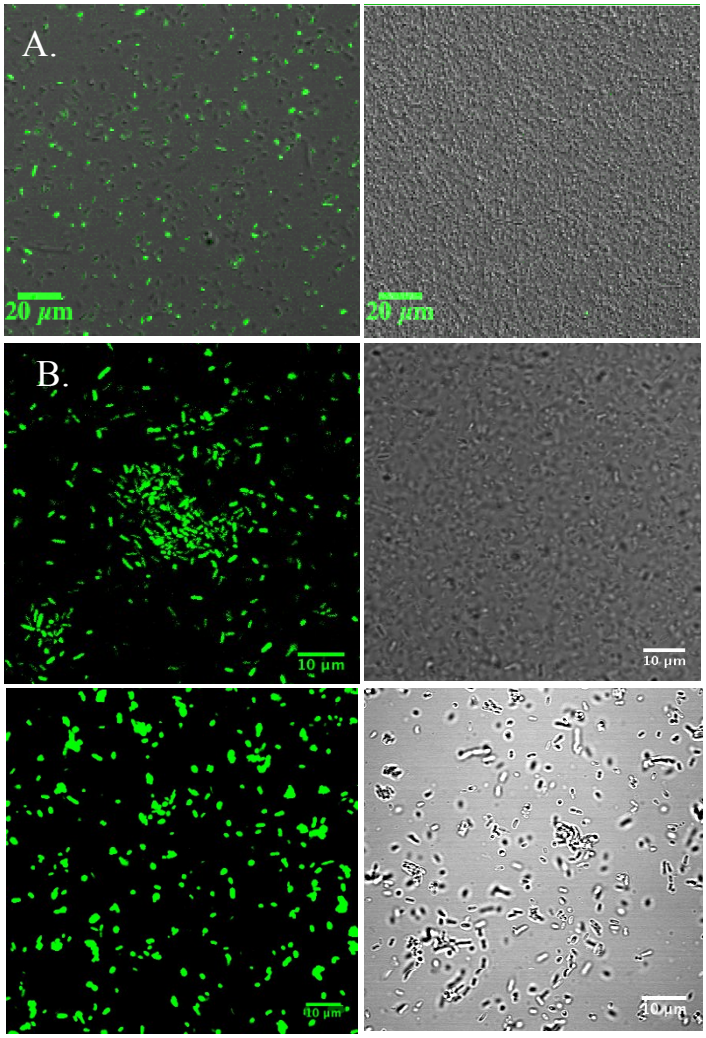


Figure 2.11. A. pPROBE:*UDP*_promoter in WT background (left) and *rcsA:*Tn5 background (right) in an ON culture of LB. B. pPROBE:*UDP*_promoter in WT background (left) and *rcsA:*Tn5 background (right) in a biofilm on a glass slide. C. pPROBE:*UDP*_promoter in WT background (left) and *rcsA:*Tn5 background (right) in a pellicle

Table 2.1. Genes downregulated in *rcsA:*Tn5 compared to WT *Pantoea* sp. YR343. grown overnight in R2A media. We generated the expression matrix using DESeq2 in KBase and filtered with a log2_fold_change cutoff of 2 and q-value (corrected p-value) of 0.05.

Locus Tag	**Function**	**log2_fold_ change**	**q_value**
PMI39_00663	Transcriptional regulator, contains XRE-family HTH domain	-2.107162657	1.48E-71
PMI39_01663	sulfite reductase (NADPH) hemoprotein beta-component	-4.261941474	1.39E-173
PMI39_02423	Putative intracellular protease/amidase	-3.191299845	2.20E-22
PMI39_02424	Pimeloyl-ACP methyl ester carboxylesterase	-2.617944738	1.54E-25
PMI39_02686	cationic peptide transport system permease protein	-3.837247046	2.92E-93
PMI39_03158	Zn-binding Pro-Ala-Ala-Arg (PAAR) domain-containing protein, incolved in TypeVI secretion	-5.127841044	1.99E-05
PMI39_03410	lycopene beta-cyclase	-3.256130494	0.01144029
PMI39_04333	peptide/nickel transport system permease protein	-4.029654168	0.00257769

Table 2.2. Genes upregulated in *rcsA:*Tn5 compared to WT *Pantoea* sp. YR343. grown overnight in R2A media. We generated the expression matrix using DESeq2 in KBase and filtered with a log2_fold_change cutoff of 2 and q-value (corrected p-value) of 0.05.

Locus Tag	**Function**	**log2_fold_ change**	**q_value**
PMI39_00792	aspartate aminotransferase family protein	2.048881451	3.47E-05
PMI39_01239	tellurium resistance protein TerA	11.20510372	0
PMI39_01330	nitrogen regulatory protein P-II 2	2.402998495	7.14E-36
PMI39_01659	siroheme synthase	2.114937676	9.48E-28
PMI39_02095	hypothetical protein	3.574202519	1.52E-135
PMI39_02096	arginase	2.245044922	1.51E-41
PMI39_02690	hypothetical protein	2.169543624	3.77E-45
PMI39_03091	succinate--CoA ligase subunit beta	9.880784011	0
PMI39_03297	thiosulfate transporter subunit	2.396874835	2.33E-44
PMI39_03960	glycine/betaine ABC transporter substrate-binding protein	2.128723495	1.76E-08
PMI39_04035	molybdate ABC transporter permease	2.918890676	0.01361531
PMI39_04198	CysB family transcriptional regulator	2.654696814	5.68E-64
PMI39_04350	MFS transporter	2.182657969	0.00011873
PMI39_04401	sulfate transporter subunit	2.412998941	3.73E-32
PMI39_04468	glutamine synthetase	2.105991926	1.85E-11
PMI39_05000	non-ribosomal peptide synthetase	2.428067482	2.15E-13
PMI39_05003	ferrichrysobactin receptor	2.083713584	0.00038907

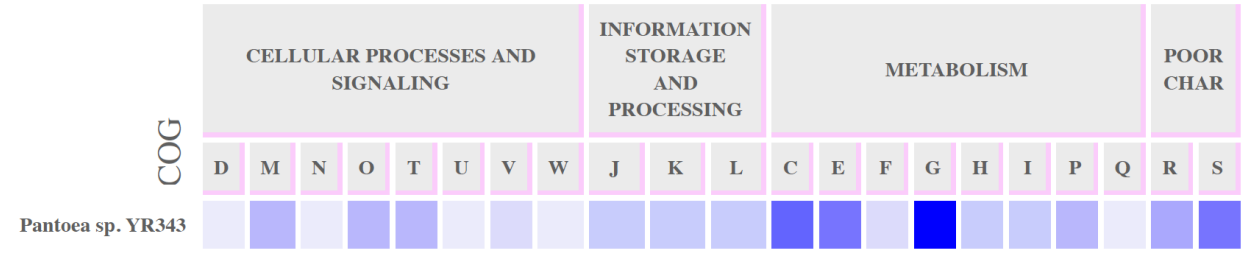


Figure 2.12. Heatmap of gene functions upregulated in the *rcsA:*Tn5 mutant compared to WT *Pantoea* sp. YR343 grown as pellicles. Darker colors correlate with increased number of genes with predicted COGs in each category. Category key is in Figure 2.14.

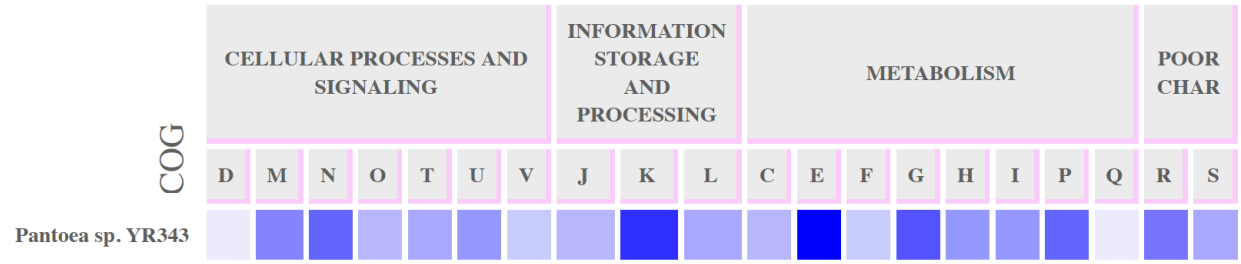


Figure 2.13. Heatmap of gene functions downregulated in the *rcsA:*Tn5 mutant compared to WT *Pantoea* sp. YR343 grown as pellicles. Darker colors correlate with increased number of genes with predicted COGs in each category. Category key is in Figure 2.14.

KEY

CELLULAR PROCESSES AND SIGNALING	D	Cell cycle control, cell division, chromosome partitioning
	M	Cell wall/membrane/envelope biogenesis
	N	Cell motility
	O	Post-translational modification, protein turnover, and chaperones
	T	Signal transduction mechanisms
	U	Intracellular trafficking, secretion, and vesicular transport
	V	Defense mechanisms
	W	Extracellular structures
	Y	Nuclear structure
	Z	Cytoskeleton
INFORMATION STORAGE AND PROCESSING	A	RNA processing and modification
	B	Chromatin structure and dynamics
	J	Translation, ribosomal structure and biogenesis
	K	Transcription
	L	Replication, recombination and repair
METABOLISM	C	Energy production and conversion
	E	Amino acid transport and metabolism
	F	Nucleotide transport and metabolism
	G	Carbohydrate transport and metabolism
	H	Coenzyme transport and metabolism
	I	Lipid transport and metabolism
	P	Inorganic ion transport and metabolism
	Q	Secondary metabolites biosynthesis, transport, and catabolism
POOR CHAR	R	General function prediction only
	S	Function unknown

Figure 2.14. Category key for heatmap of predicted COG functions in Figures 2.12-13.

The absence of a capsule for *rcsA:*Tn5 indicates a defect in EPS production. Moreover, we determined that the EPS from *rcsA*:Tn5 differs from WT in that it is reduced in galactose, glucose, and glucuronic acid based on monosaccharide analyses. Interestingly, these are key residues in the structure of stewartan and amylovoran[64], and suggest that *Pantoea* sp. YR343 may produce a structurally similar EPS. Functionally, these changes in EPS abundance and composition in *rcsA*:Tn5 resulted in defects in biofilm and pellicle formation, as well as in plant colonization. That the colonization defect of *rcsA*:Tn5 could be rescued by co-culture with WT cells suggests that the WT cells are providing some molecule or function that influences *rcsA*:Tn5 colonization efficiency. Based on our results, it is possible that the production of EPS by WT cells may promote the formation of mixed biofilms on plant roots.

In the same genetic screen that identified *rcsA*:Tn5, we also isolated a transposon mutant for PMI39_01848 or *UDP*. It is notable that the monosaccharide composition between *rcsA:*Tn5 and *UDP:*Tn5 are similar. This could indicate a regulatory connection between the two, which is further emphasized by the promoter studies. That the *UDP* promoter is not active in the *rcsA:*Tn5 background suggests that RcsA regulates *UDP* gene expression, although whether this regulation is direct or indirect is currently unknown. This result aligns with the studies by Burke et al., 2015, in which undecaprenyl-phosphate UDP-galactose phosphotransferase (*wceG2*), which is a homolog of PMI39_01848, is activated by RcsA in *P. stewartii*. *WceG2* and *UDP* could be regulated similarly in both strains.[3]

We determined the full regulon of RcsA to identify other possible contributors to EPS production and colonization in *Pantoea* sp. YR343. We found that *UDP* is significantly downregulated in the *rcsA:*Tn5 mutant compared to the WT when grown as a pellicle. Other genes in the cluster in *Pantoea* sp. YR343 (PMI39_01835-1848) that is predicted to encode proteins homologous to those involved in stewartan production were also downregulated, including PMI39_01847, PMI39_01846, and PMI39_01838. This suggests that RcsA may regulate EPS production primarily by activating the cluster containing *UDP*. The promoters for *rcsA* and *UDP* are both expressed during growth in LB medium, colonization on plant chambers, and biofilm and pellicle formation.

The different *rcsA:*Tn5 Congo Red phenotypes with and without the presence of c-di-GMP and the partial rescue of the *rcsA*:Tn5 pellicle defect with high c-di-GMP indicate a

possible regulatory connection between RcsA and c-di-GMP.[7] A gene encoding a diguanylate cyclase (PMI49_00995), which drives the synthesis of c-di-GMP, is downregulated in *rcsA:*Tn5 compared to the WT when grown as a pellicle. In addition, a gene encoding a phosphodiesterase (PMI39_01056), which synthesizes the degradation of c-di-GMP, is upregulated in *rcsA:*Tn5 compared to the WT when grown as a pellicle. This indicates that RcsA plays a positive role in the production of c-di-GMP.

In *Pantoea stewartii,* RcsA is repressed at low cell densities through a quorum sensing regulatory mechanism involving a LuxR homolog, EsaR.[59] *Pantoea* sp. YR343, however, does not have a homolog for *P. stewartii's* EsaR*,* suggesting that *rcsA* may be regulated differently in *Pantoea* sp. YR343. The RNASeq data shows that RcsA plays a role in the depression of N-acyl-L-homoserine lactone (AHL) synthetase, which catalyzes the production of AHL, during pellicle formation. This indicates that RcsA contributes to the downregulation of quorum sensing. It is possible that LuxR regulates quorum sensing in *Pantoea* sp. YR343 partially by regulating RcsA. Future studies are needed to determine the definite involvement of LuxR in the regulation of *rcsA* in *Pantoea* sp. YR343.

CHAPTER THREE: OTHER PROJECTS

This chapter summarizes additional projects including preliminary data on salicylate degradation and other transposon mutants isolated from the c-di-GMP screen in *Pantoea* sp. YR343. We specifically examined the transposon mutants for genes encoding the LuxR and LrhA transcription factors because we hypothesized that the LuxR homolog regulates LrhA as well as RcsA in *Pantoea* sp. YR343 (Figure 3.1).

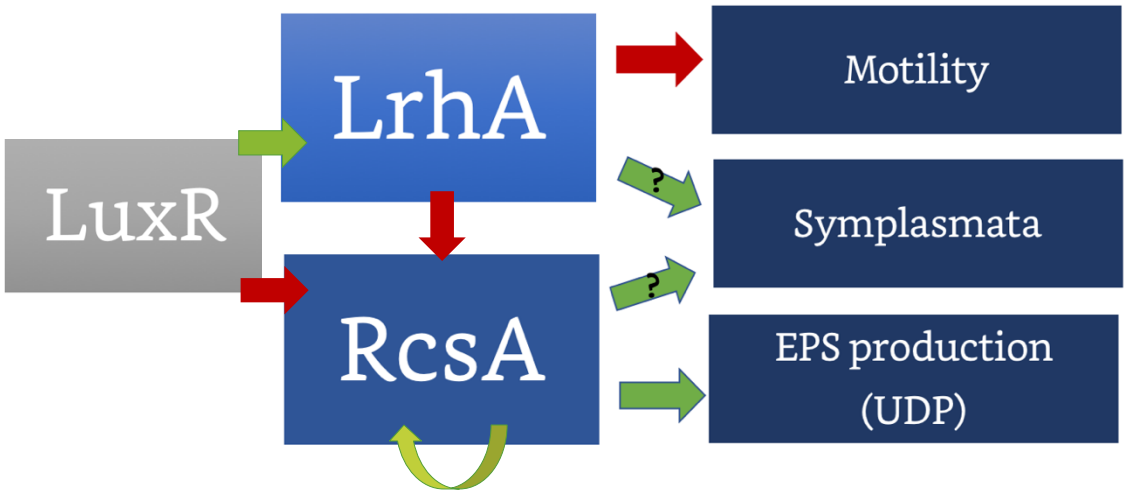


Figure 3.1. LuxR likely positively regulates LrhA and negatively regulates RcsA in *Pantoea* sp. YR343. In turn, LrhA suppresses genes with motility functions and RcsA activates genes that produce EPS, like *UDP*. In addition, both LrhA and RcsA contribute to the development of symplasmata.

We isolated *luxR*:Tn5 in our screen for genes involved in c-di-GMP. As the only LuxR homolog in *Pantoea* sp. YR343, we hypothesize that LuxR regulates *rcsA* and *lrhA* in *Pantoea* sp. YR343. We compared our LuxR homolog to other homologs in *Pantoea* strains (Table 3.1). We did not get a close match to *Pantoea stewartii's* EsaR, which is unexpected because EsaR regulates RcsA in *Pantoea stewartii.* It is possible that our homolog functions differently. We only have one homolog, while *Pantoea stewartii* contains two. There is a high percent ID between *Pantoea* sp. YR343's LuxR and the homologs in GM01, YR525, and YR512. There are two homologs in OV426, which could contribute to its slightly lower percent ID. We also found a LuxI homolog in *Pantoea* sp. YR343 that is adjacent to LuxR and determined its amino acid percent ID to other closely related species (Table 3.2).

The *luxR:*Tn5 mutant has even co-colonization with the WT, but decreased colonization when colonized by itself on the wheat roots (Chapter 2: Methods, Figures 3.3-3.4).

Table 3.1. BLAST ID and number of LuxR homologs in *Pantoea* strains compared to *Pantoea* sp. YR343 (PMI39_00509)

Pantoea Strain	**LuxR nucleotide ID**	**LuxR homologs locus tags**
Stewartii	66 % (SdiA) 26 % (EsaR)	CKS_4147 CKS_2903
GM01	95 %	PMI17_01419
YR525	100 %	Ga0115490_101468
YR512	100 %	Ga0115489_101468
OV426	71 %	Ga0115488_2481 Ga0115488_1611

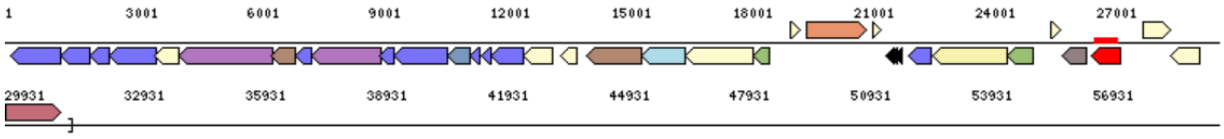


Figure 3.2. Gene neighborhood of LuxR adjacent to LuxI (PMI39_00508) in *Pantoea* sp. YR343.

Table 3.2. BLAST ID and number of LuxI homologs in *Pantoea* strains compared to *Pantoea* sp. YR343 (PMI39_00509)

Pantoea Strain	**LuxI nucleotide percent ID**	**LuxI homolog locus tag**
Stewartii	86.63%	NZ_AHIE01000008
GM01	99.01%	PMI17_GM01_CGATGT_L007_R1_006_paired_trimmed_paired_contig_61.61
YR525	100%	Ga0115490_101
YR512	100%	Ga0115489_101
OV426	87.68%	Ga0115488_101

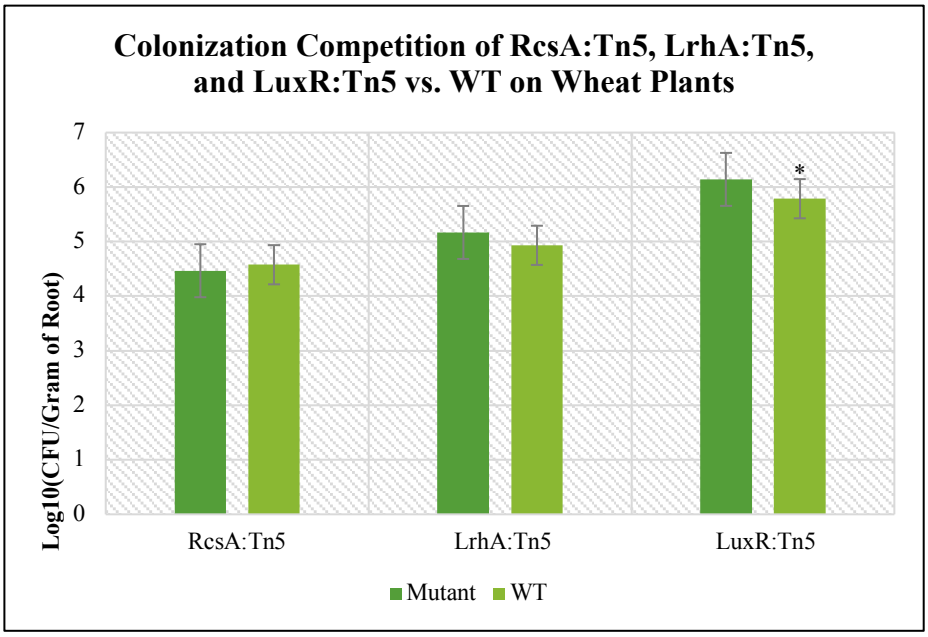


Figure 3.3. Colonization of *rcsA:*Tn5, *lrhA:*Tn5, and *luxR:*Tn5 inoculated with WT *Pantoea* sp. YR343 on wheat roots. Error bars determined by standard error. Bars are the mean of three to four replicates per strain. *p-value<0.5 determined by T-test.

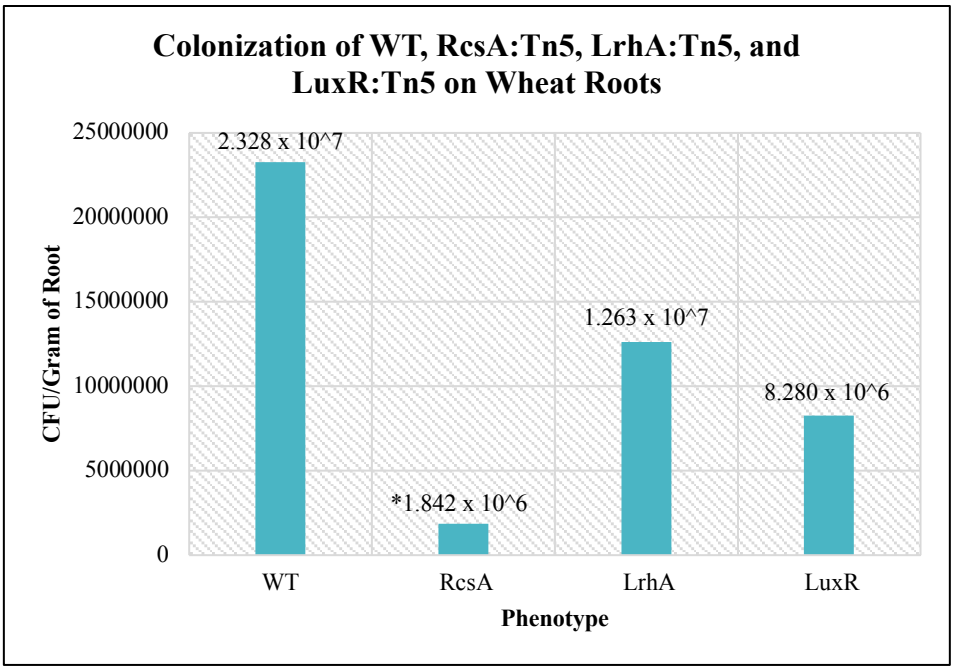


Figure 3.4. Colonization of *rcsA:*Tn5, *lrhA:*Tn5, and *luxR:*Tn5 inoculated on individual wheat roots. Error bars determined by standard error. Bars are the mean of three to four replicates per strain. *p-value<0.5 determined by T-test.

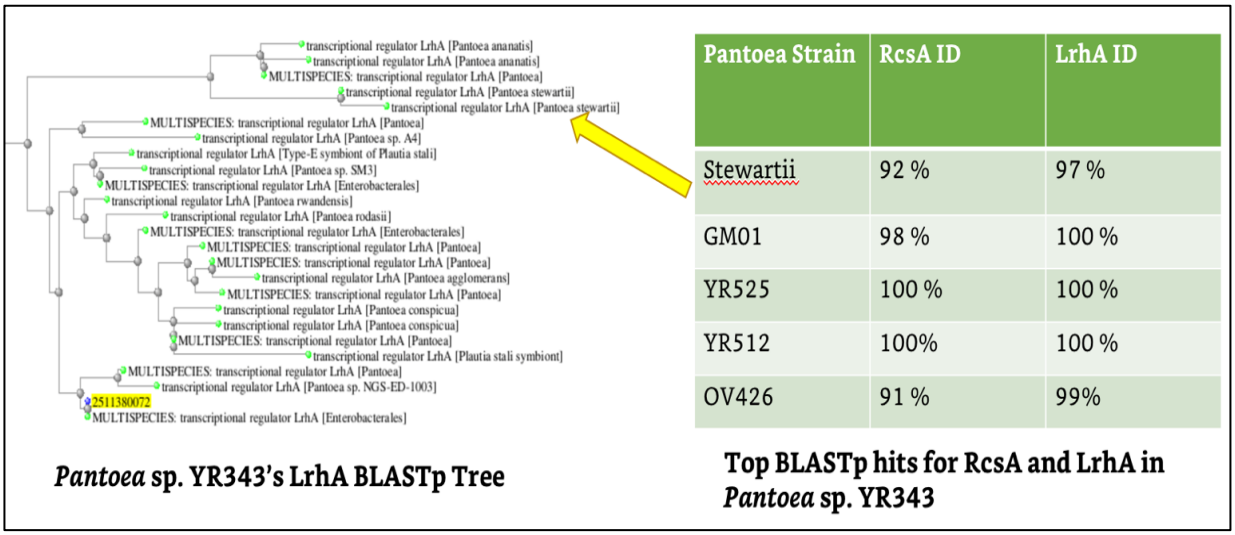
LrhA: A Transcription Factor

LrhA most likely affects swarming in *Pantoea* sp. YR343. Swarming motility is an infamous characteristic of the plant pathogen, *P. stewartii. P. stewartii* shows enhanced swarming motility in glucose, while *Pantoea* sp. YR343 shows enhanced swarming in glycerol. This indicates a possible difference in metabolism.[1] Hyperflagellated swarm cells undergo coordinated population migration across a solid surface. Critical stimuli include cell density, surface contact, and physiological signals, such as anaerobicity. Mass translocation is facilitated by close cell alignment and production of secreted migration factors. Swarming allows bacteria to rapidly colonize nutrient-rich environments, which accelerates biomass production and would allow increased colonization in the rhizosphere.[66, 67]

We created a BLASTp tree LrhA comparing the IDs from *Pantoea* sp. YR343 to different Pantoea strains (Figure 3.5). This showed close sequence conservation between strains.

In our swarming assay, overnight cultures of the WT, *lrhA*:Tn5, and pSRK:*lrhA* were diluted to an OD_{600} of 0.05 in LB broth and grown to an OD_{600} of 0.5. 5 µL of this culture was

spotted onto the agar surface of LB 0.6% agar plates poured the same day. *LrhA*:Tn5 swarming covered an even/slightly more surface area compared to the WT, while the overexpression mutant had a decrease in surface area covered compared to the WT (Figure 3.6 A). This is in contrast to the swarming phenotype seen by Burke et al. in *P. stewartii.* The biofilm assay also showed a decrease in biofilm formation for *lrhA*:Tn5 compared to WT (Figure 3.6 B). Swarming occurs on the colony level, which is unlike the cellular-level of biofilm formation.[68] This could indicate LrhA has a broad regulatory influence in *Pantoea* sp. YR343. There was a drop in colonization cell counts of *lrhA*:Tn5 (1.263x10^7 log10 CFU/gram) compared to WT (2.328x10^7 log10 CFU/gram), but it was not significant. These data suggest that LrhA may negatively regulate swarming behavior.



Pantoea Strain	RcsA ID	LrhA ID
Stewartii	92 %	97 %
GM01	98 %	100 %
YR525	100 %	100 %
YR512	100%	100 %
OV426	91 %	99%

Top BLASTp hits for RcsA and LrhA in *Pantoea* sp. YR343

Figure 3.5. A. BLASTp tree of transcription factor LrhA in *Pantoea* sp. YR343. B. BLASTp top hits for RcsA and LrhA in *Pantoea* sp. YR343. Yellow arrow indicates the location of the *Pantoea stewartii* LrhA homolog in the BLASTp tree.

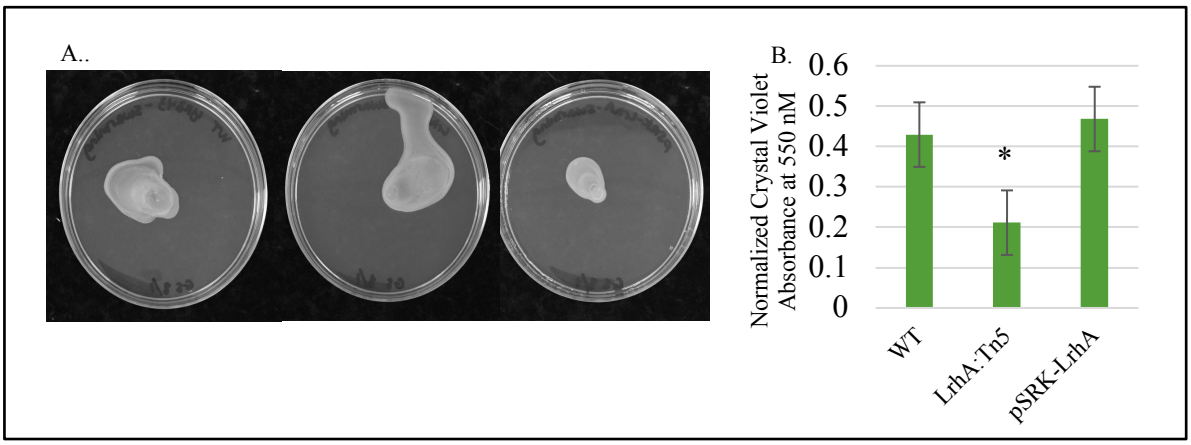


Figure 3.6. LrhA phenotypes. A. Swarming assay of WT, *lrhA*:Tn5, pSRK:*lrhA*. B. Crystal violet biofilm assay.

Symplasmata

The *rcsA*:Tn5 and *lrhA*:Tn5 mutants form no/few evident symplasmata, while WT *Pantoea* sp. YR343 contain hundreds in a single pellicle. Symplasmata contain several to hundreds of bacterial cells inside a shared capsule and have been shown to confer tolerance to stress (Figure 3.7). We developed a method to image and quantify symplasmata in *Pantoea* sp. YR343 (Figure 3.8-3.11). This method could be applied to colonization studies and could further characterize the role of LrhA and RcsA and their contribution to symplasmata in *Pantoea* sp. YR343.

These studies could be expanded by analyzing symplasmata development, its role in colonization, formation under stress and in different medias. These could be done with time scales and using the *rcsA:*Tn5 and *lrhA:*Tn5 mutants.

*LrhA:*Tn5 does not form symplasmata in *Pantoea eucalypti* 299R (Figure 3.12).[5] *LrhA:*Tn5 in *Pantoea* sp. YR343 also does not form symplasmata (Figure 3.12). *RcsA:*Tn5 in *Pantoea* sp. YR343 clusters like symplasmata but does not form a capsule (Figure 3.14).

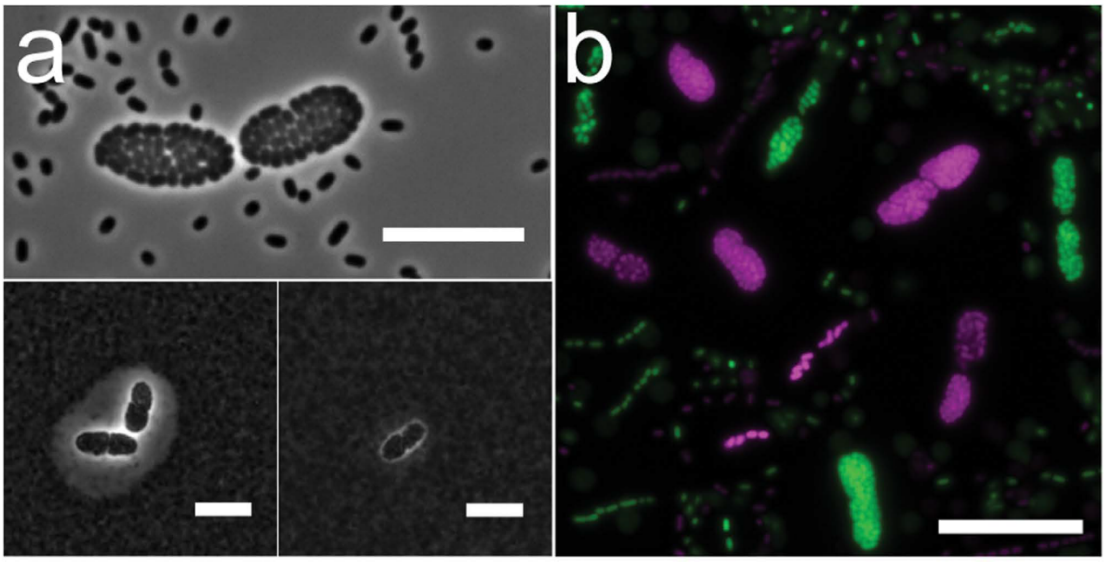


Figure 3.7. *Pantoea eucalypti* 299R form symplasmata. A. Phase-contrast image showing pair of symplasmata (top). Counter-staining with Indian ink reveals capsule surrounding cells (bottom). B. Cells expressing either GFP or DsRed depicting clonal tendency of symplasmata. Bar = 20 um.[5]

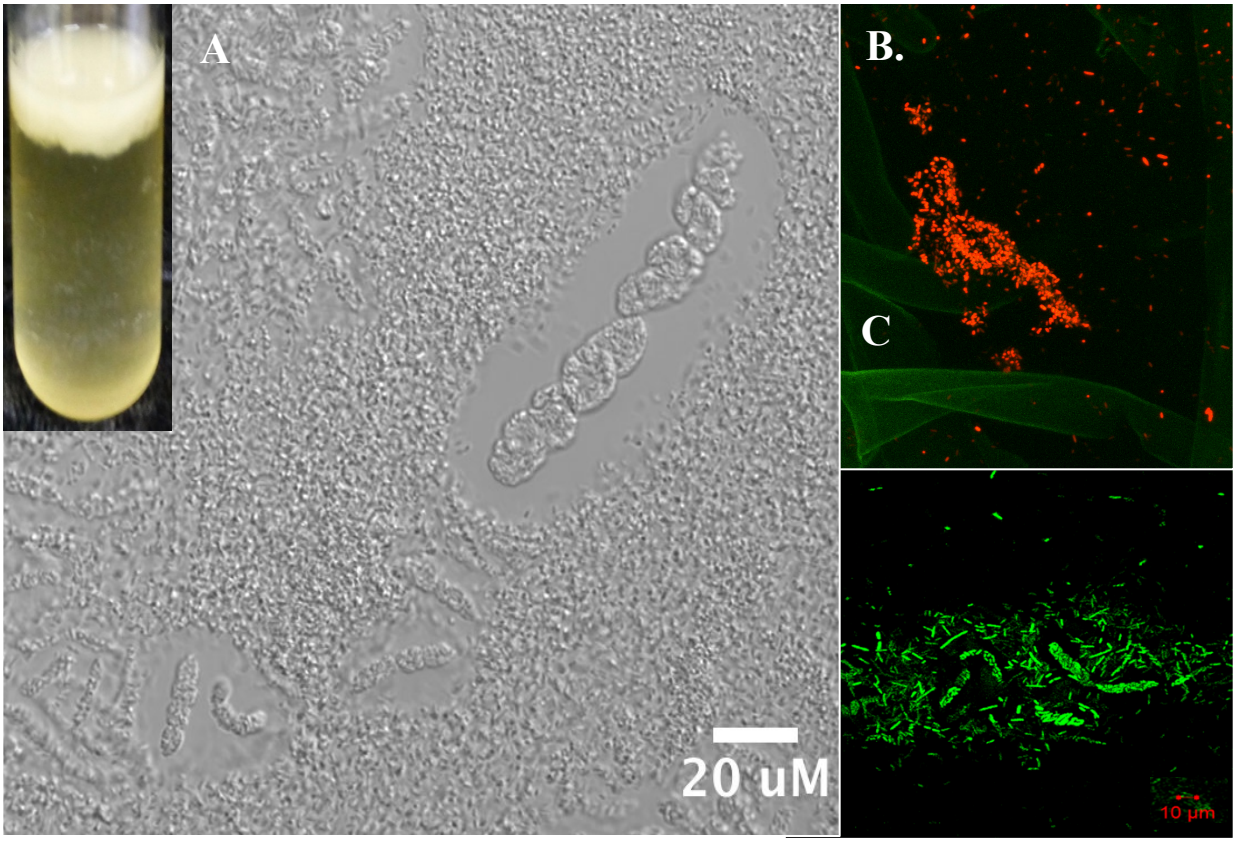


Figure 3.8. *Pantoea* sp. YR343 form symplasmata. A. Pellicles contain abundant symplasmata. Brightfield image of symplasmata of various sizes. B. Symplasmata formation on wheat roots of *Pantoea* sp. YR343 with mcherry fluorescence. C. GFP *Pantoea* sp. YR343 colonies from a pellicle.

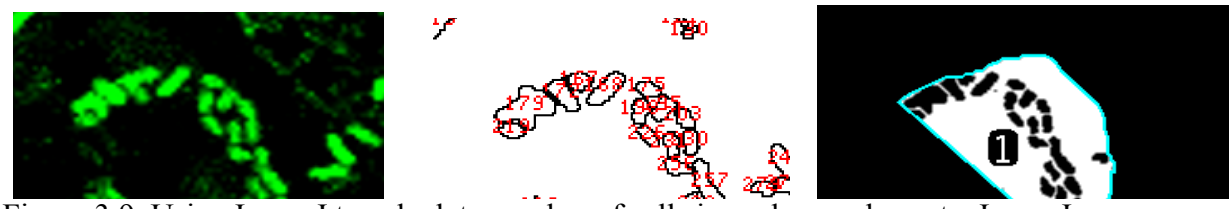


Figure 3.9. Using ImageJ to calculate number of cells in each symplasmata. ImageJ can separate the fluorescent cells and watershed to account for error. The new image (right) can be used to count the individual cells.

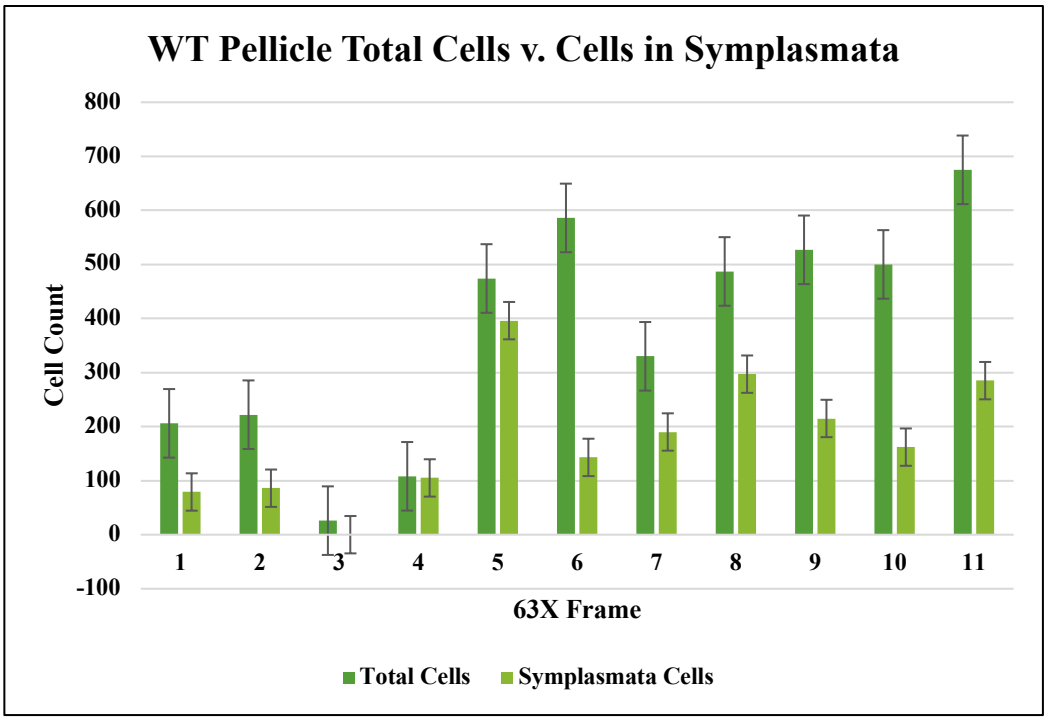


Figure 3.10. Using ImageJ to calculate number of cells in each symplasmata in WT *Pantoea* sp. YR343. Bars represent total cells. Error bars are standard error.

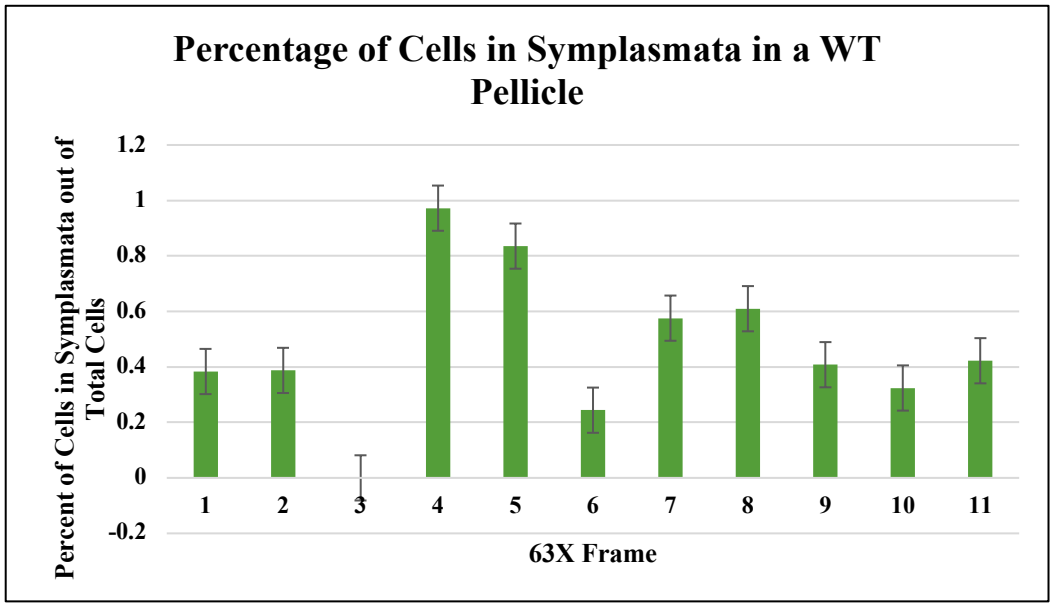


Figure 3.11. Using ImageJ to calculate number of cells in each symplasmata as a percentage of symplasmata vs. total cells in WT *Pantoea* sp. YR343. Bars are a percentage of cells. Error bars are standard error.

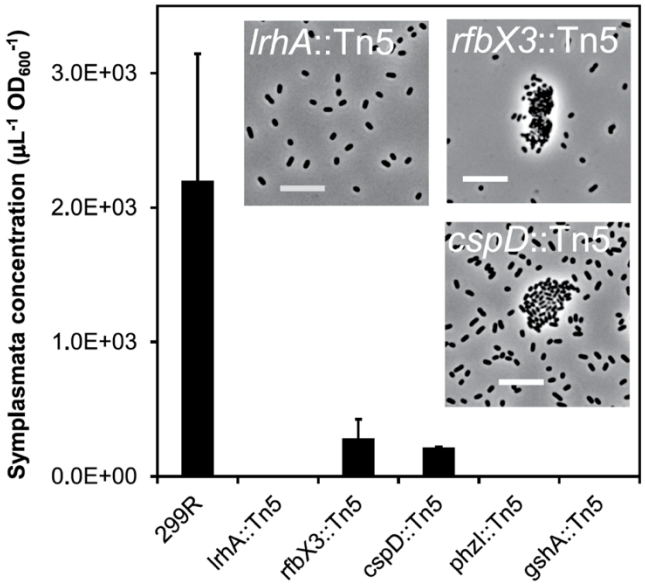


Figure 3.12. WT and transposon mutant symplasmata formation of *Pantoea eucalypti* 299R. *LrhA:*Tn5 does not form symplasmata.[5]

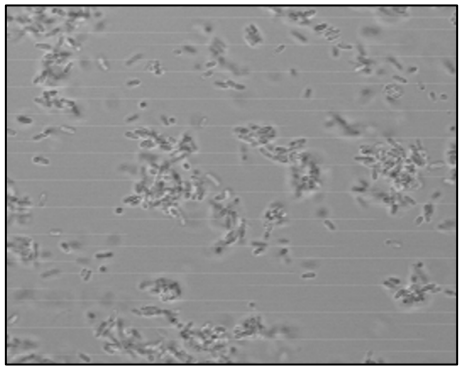


Figure 3.14. *RcsA:*Tn5 clusters with no capsule in a pellicle.

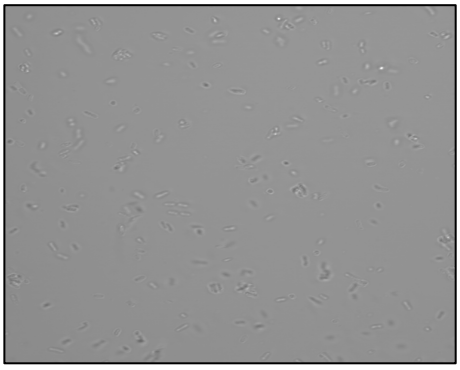


Figure 3.13. *LrhA:*Tn5 does not form symplasmata in a pellicle.

One of the transposon mutants also isolated in the c-di-GMP screen encoded a predicted DNA helicase known as PMI39_00093 and in a gene neighborhood with membrane proteins(Figures 3.15-3.16). Interestingly, the mutant showed similar phenotypes to *rcsA:*Tn5. The mutant does not have a pellicle defect like *rcsA:*Tn5, but does have a biofilm defect and trypan blue phenotype, which indicates a role in EPS production (Figures 3.17-3.19). PMI39_00093 is not significantly up or downregulated in the RNASeq analysis for *rcsA:*Tn5 (Chapter 2: Results). Future experiments could explore how PMI39_00093 is regulated, affects EPS production, and relates to c-di-GMP.

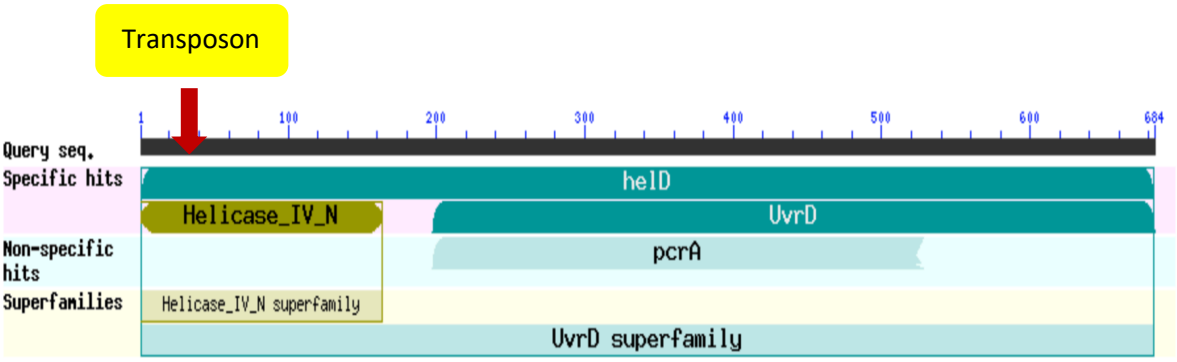


Figure 3.15. Depiction of transposon insertion into the gene encoding DNA helicase using BLAST.

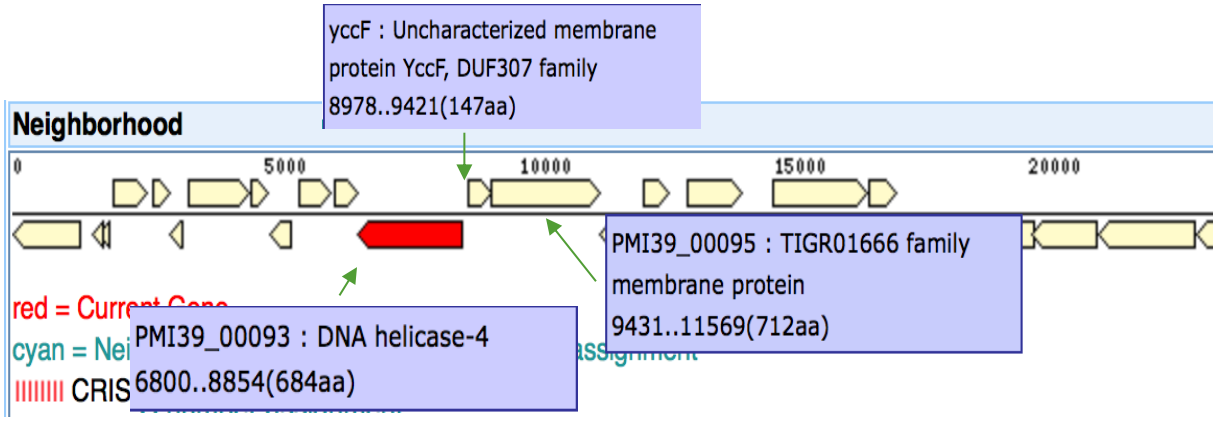


Figure 3.16. Location of PMI39_00093 using IMG with descriptions of adjacent genes.

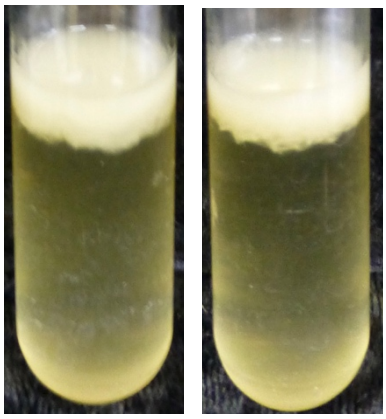


Figure 3.17. Similar pellicle formation for WT (left) and BB4 (right).

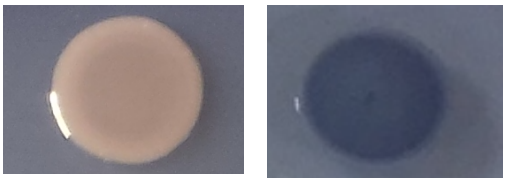


Figure 3.18. Trypan blue phenotype for BB4 (right) compared to WT (left).

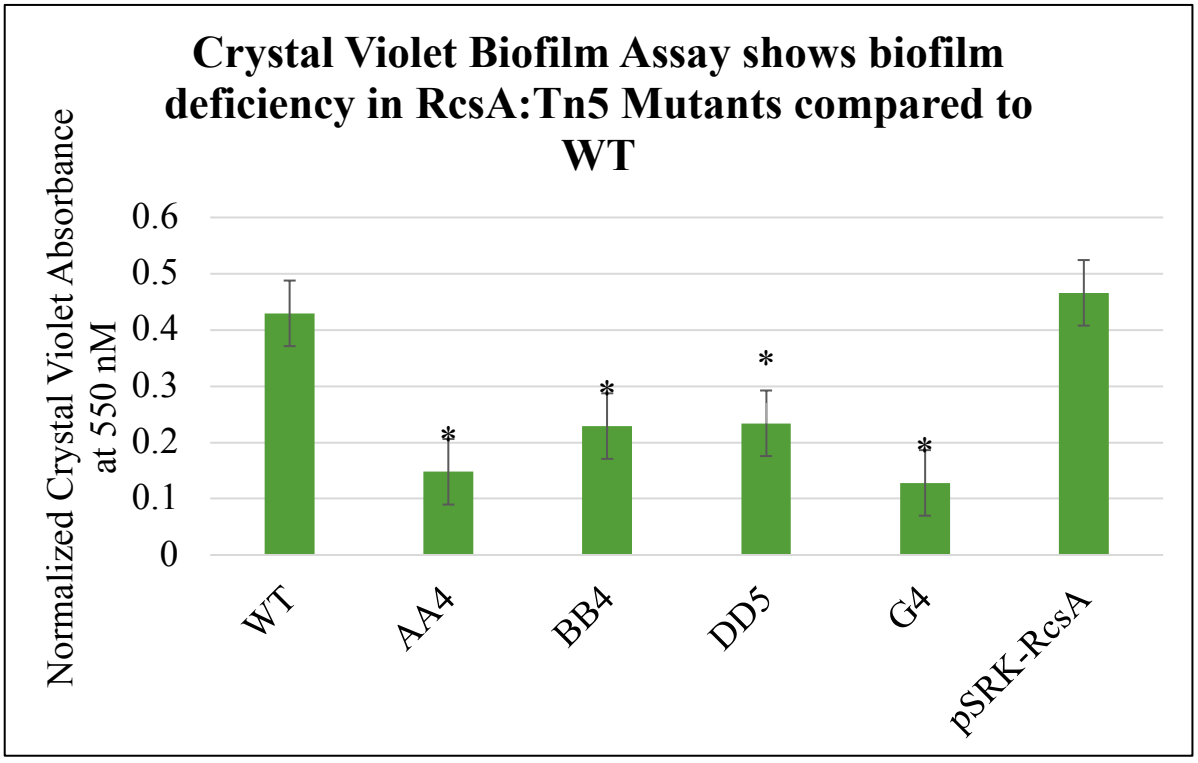


Figure 3.19. Significant biofilm defect for BB4 compared to WT *Pantoea* sp. YR343 in a crystal violet biofilm assay. *p-value<0.5 determined by T-test. Bars are a mean of six replicates. Error bars are standard error.

Diguanylate phosphodiesterase catalyzes the degradation of cyclic c-di-GMP to monophosphate (GMP; Figure 3.20). We identified a transposon insertion into a gene predicted to encode a diguanylate phosphodiesterase in *Pantoea* sp. YR343, PMI39_00827, labeled G11. The deoxyguanosinetriphosphate triphosphohydrolase (dGTPase), PMI39_03698, is labeled G7 and is also involved in c-di-GMP synthesis because it hydrolyzes dGTP to deoxyguanosine. We conducted preliminary growth, biofilm, pellicle, and swimming assays to determine possible phenotypes of the transposon mutants related to c-di-GMP.

G11 grows similarly to WT *Pantoea* sp. YR343. There is no significant biofilm defect in a crystal violet assay, but G11 does not form as solid of a pellicle as WT. There is a definite swimming defect for G11 compared to the WT (Chapter 2: Methods, Figures 3.21-3.24).

G7 also grows similarly to the WT. It does not have a significant biofilm, pellicle, or motility phenotype (Chapter 2: Methods, Figures 3.21-3.23).

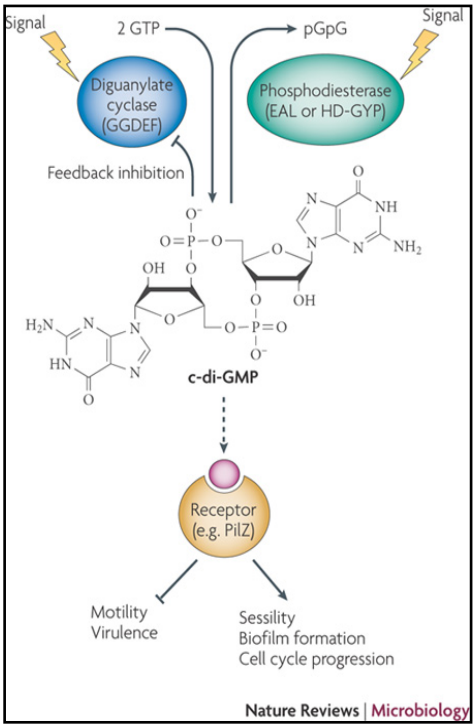


Figure 3.20. Degradation of c-di-GMP by a diguanylate phosphodiesterase.

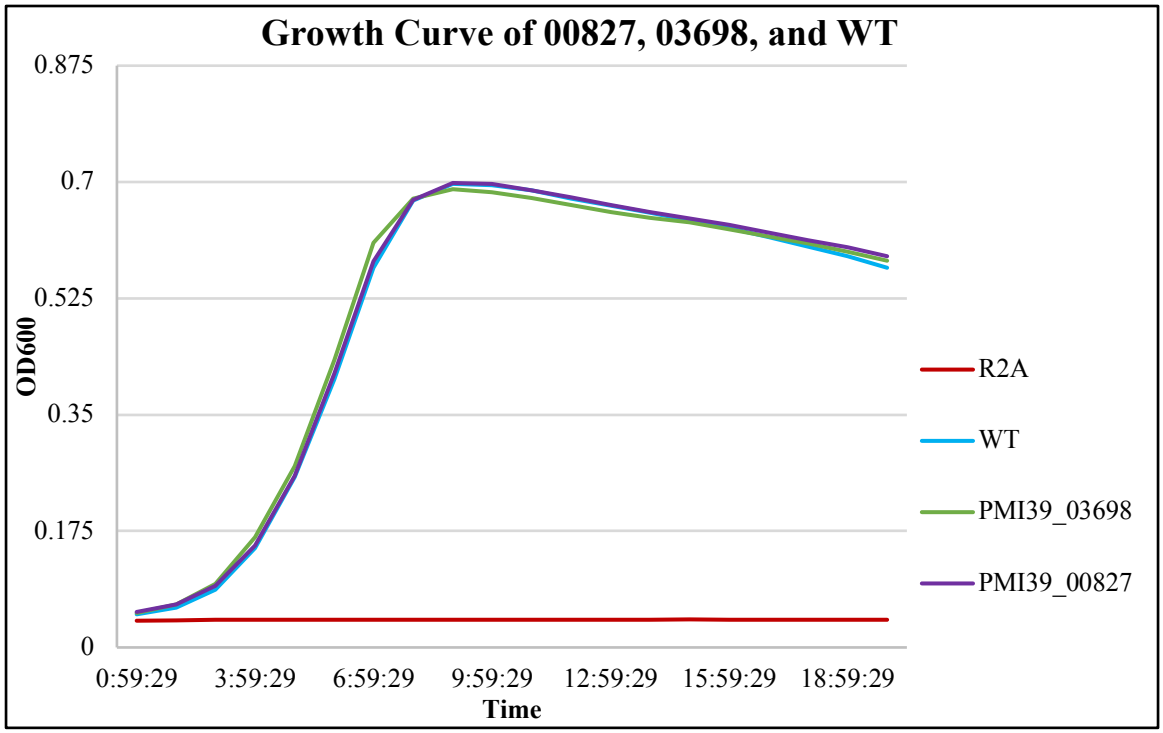


Figure 3.21. Equal growth of transposon mutants compared to WT.

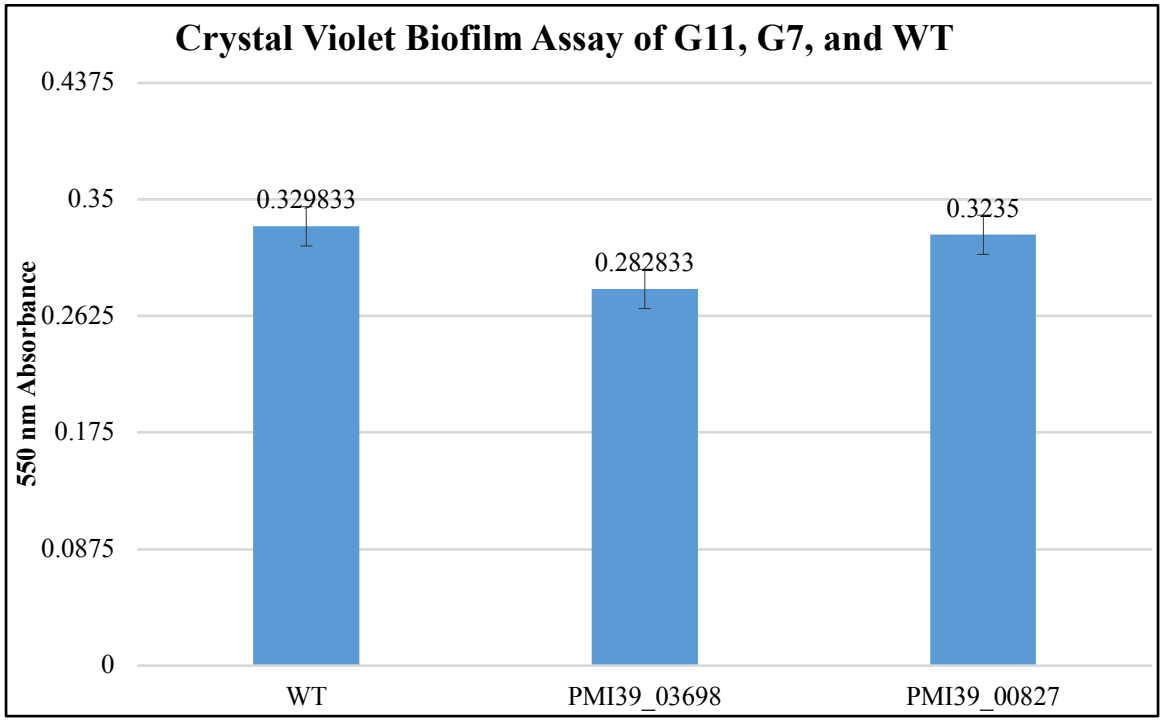


Figure 3.22. Equal biofilm development of transposon mutants compared to WT. Error bars are standard error. Bars are a mean of six replicates.

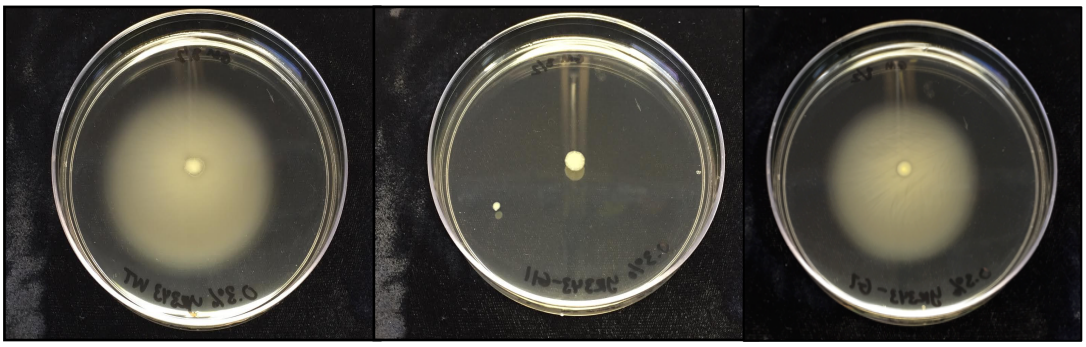


Figure 3.23. Swimming motility for WT (left), G11 (center), and G7 (right).

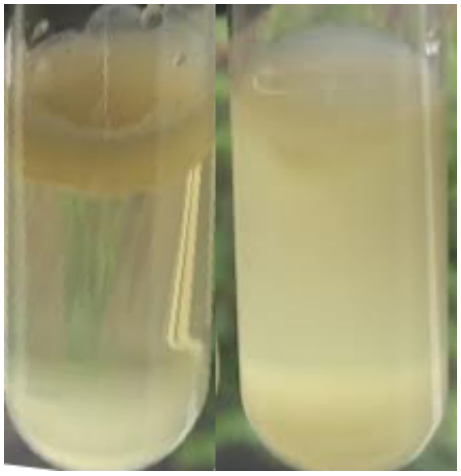


Figure 3.24. Pellicle defect for G11 (right) compared to WT (left).

Salicin Degradation

Populus trees host a large microbial community in the rhizosphere. It produces secondary metabolites known as higher-order salicylates (HOS). We wanted to determine how HOS affects the host-microbiome composition and physiology. We performed initial studies with glucose and salicin as carbon sources to test the growth of *Pantoea* sp. YR343 in the presence of HOS. We examined the growth of *Pantoea* sp. YR343 in the presence of salicin and glucose on 96-well plates. We grew ON cultures in the presence and absence of salicin or glucose. Next, we inoculated the ON cultures into fresh media with or without salicin or glucose in a 96-well plate (Figure 3.25). The "Blank" samples were uninoculated. The salicin to salicin cultures had little to no growth and the glucose to salicin cultures had delayed growth. This inspired the following questions and experiments.

1. Is salicylate by-product toxic? Yes. There is no growth of *Pantoea* sp. YR343 in the presence of salicylate and salicin, salicin and glucose, and only salicylate (Figure 3.26).
2. Does evaporation in a 96-well plate result in toxic concentrations of salicin/salicylate? Evaporation in a 96-well plate does result in toxic concentrations. Overnight growth of 250 mL cultures showed growth of salicin (1.1mL 50mM salicin/10 mL media) to salicin cultures. Note that the cultures did not reach as high of an OD as the glucose (1 mL 20% glucose/50 mL media) cultures (Figure 3.27-3.28).
3. Is there limited survivability of *Pantoea* sp. YR343 in salicin? ATP/OD readings indicate live cells and showed no evidence of limited survivability in the presence of salicin (Table 3.3).

We also created a family tree for Glycoside hydrolase family genes because aryl-β-glucosidase activity is induced in the presence of salicin in *Pantoea* sp. YR343 (Figure 3.29).

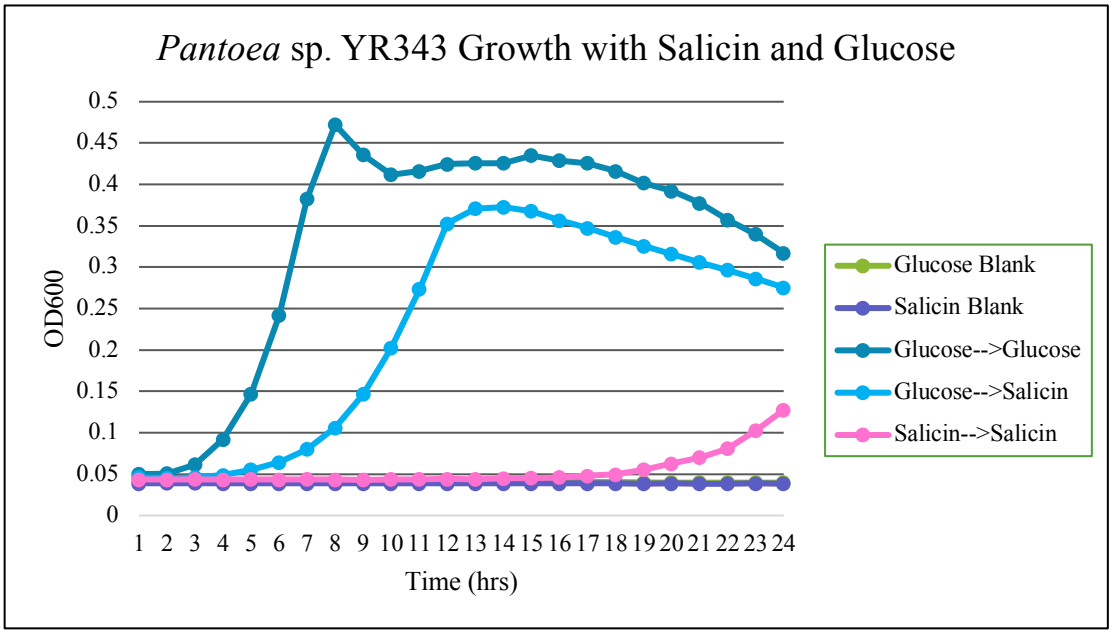


Figure 3.25. Growth in a 96-well plate. Little to no growth for salicin to salicin cultures and delayed growth for glucose to salicin cultures.

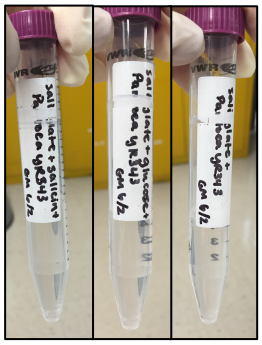


Figure 3.26. R2A cultures showing no growth.

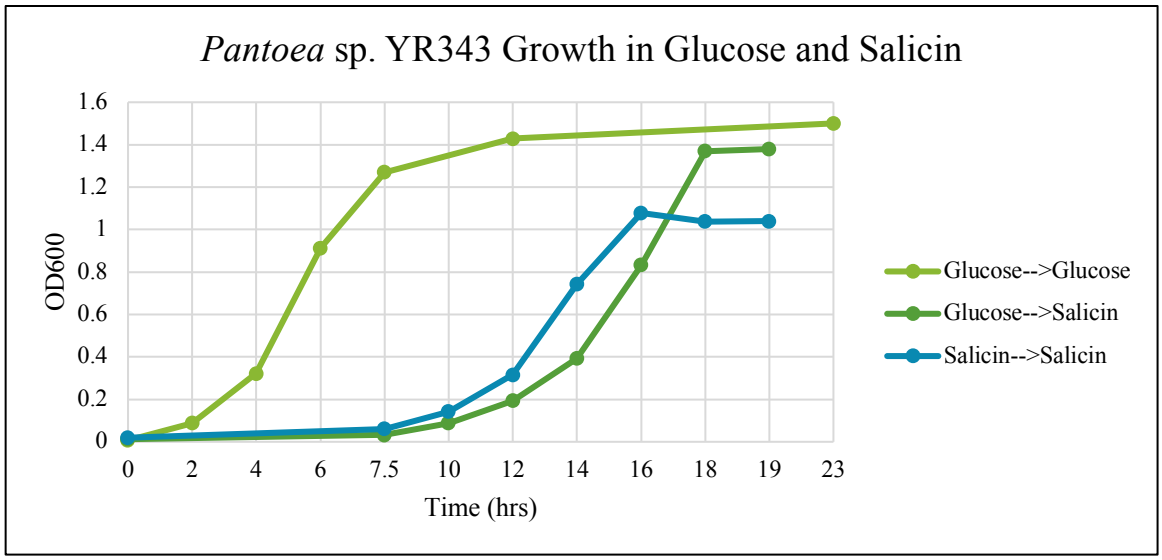


Figure 3.27. Growth in 250 mL of MOPS. Delayed and slightly reduced growth for salicin to salicin cultures and delayed growth for glucose to salicin cultures.

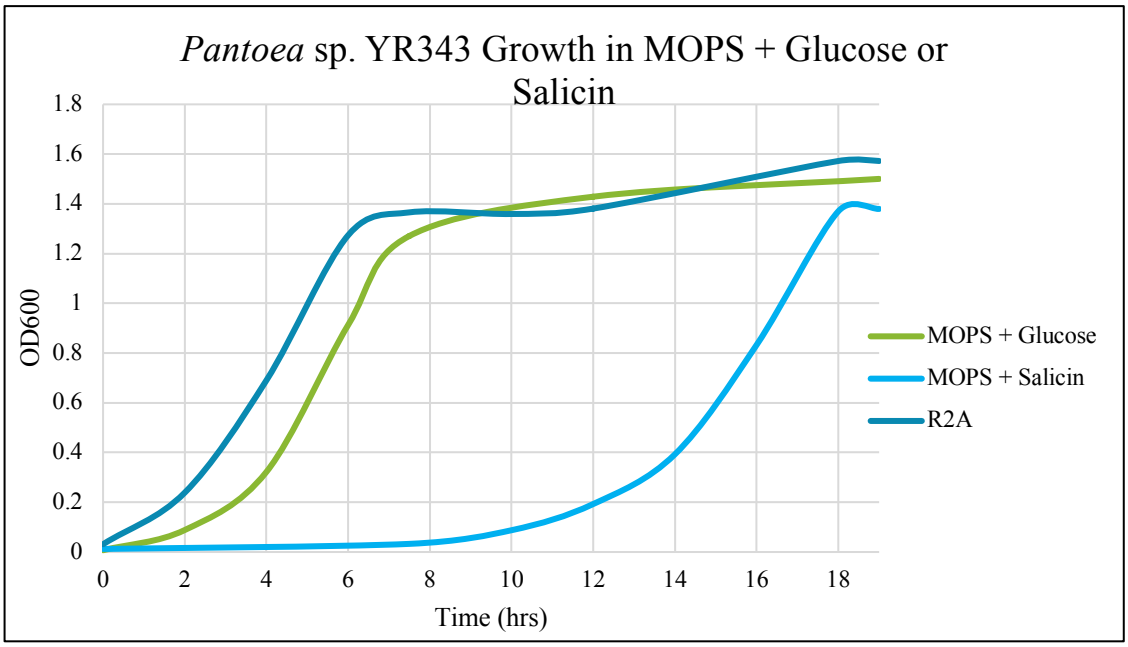


Figure 3.28. Growth in 250 mL of MOPS with glucose or salicin compared to cultures grown in R2A. MOPS + glucose grows similarly to R2A, but MOPS + salicin has delayed growth of about 12 hrs.

Table 3.3. ATP/OD readings show no significant differences. Testing the supernatant alone rendered no ATP reading, so salicylate does not contribute to the results.

Condition	OD600	ATP Reading*	ATP/OD
Glucose→Glucose	0.9129	542929.65	594730.693
Glucose→Salicin	1.3699	755344.3333	551386.476
Salicin→Salicin	1.0381	611116.3333	588687.345

Four glycoside hydrolase family 1 enzymes encoded in *Pantoea* sp. YR343

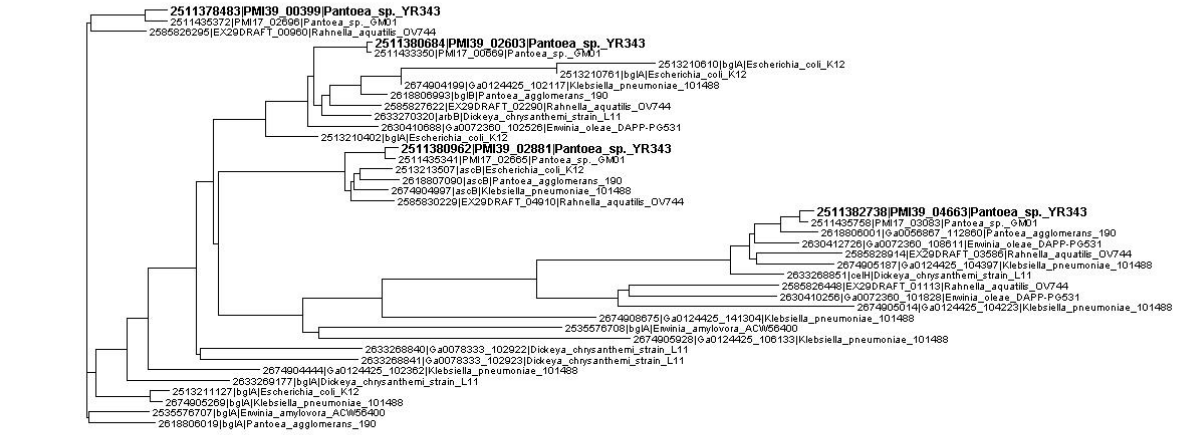


Figure 3.29. Comparing Glycoside hydrolase family 1 genes. Aligned using TCoffee, formatted into a Newick file using Clustal W2, and viewed and edited using Dendroscope.

Transport Transposon Mutants

This section provides an overview of eight transposon mutants isolated by the c-di-GMP screen. They had predicted functions for a glycerol kinase (PMI39_04394), glycerol uptake facilitator (PMI39_04393), D-xylose substrate binding (PMI39_02071), glyceraldehyde 3-phosphate dehydrogenase (PMI39_03169), substrate-binding ABC (PMI39_04218), hydroxymethlypyrmidine substrate-binding (PMI39_04978), and L-ribulose-5-phosphate 4-epimerase (PMI39_02700). We selected these mutants for further studies because they had predicted functions related to transport in *Pantoea* sp. YR343.

We analyzed growth, biofilm development, pellicle formation, colony counts, and previously acquired proteomic data (Tables 3.5-3.7 and Figures 3.30-3.31). We summarized these analyses in the following Table 3.4.

Table 3.4. Overview of transport mutants isolated from c-di-GMP transposon screen. "-" indicates no significant phenotypic difference from the WT.

Predicted description	PMI39_	Short ID	**Growth Curve**	**Biofilm Difference from WT**	**Pellicle Test**	**Confocal**	**Log2ratio_ GluToSal**
Glycerol kinase	04394	F12	-	0.007166	Smaller pellicle	-	-4.011092507
Glycerol uptake facilitator	04393	F11	-	0.125	Smaller pellicle that sinks	More colonies	-
D-xylose substrate binding	02071	BB5	Slightly lower peak	-0.2055	-	-	-4.876327997
Glyceraldehyde 3-phosphate dehydrogenase	03169	BB6	-	-0.132166	-	-	-1.769667321
Substrate-binding ABC	04218	BB7	Slightly lower peak	-0.153833	-	-	-
Hydroxymethlypyrmidine substrate-binding	04978	BB11	Slightly higher peak	-0.179333	Smaller pellicle	-	-0.216521144
L-ribulose-5-phosphate 4-epimerase	02700	D4	-	0.02433	-	-	-

Table 3.5. Predicting the function of transport mutants isolated from c-di-GMP transposon screen.

PMI39_	Short Experi-ment ID	IMG Description	Super Family	Protein Family	Closest BLAST hit	BLAST ID %
02071	BB5	D-xylose transport system substrate binding protein	ABC	_13407	D-xylose transporter subunit XylF [Enterobacter ludwigii]	99
02667	A9	oligopeptide transport system substrate-binding protein	ABC	_00496	oligopeptide ABC transporter substrate-binding protein OppA [Enterobacter ludwigii]	99
02700	D4	L-ribulose-5-phosphate 4-epimerase	ABC	_00596	ribulose phosphate epimerase [Enterobacter ludwigii]	99
03169	BB6	glyceraldehyde 3-phosphate dehydrogenase	Glycer-aldehyde	_00044 _02800	glyceraldehyde-3-phosphate dehydrogenase [Enterobacter ludwigii]	99
04218	BB7	branched-chain amino acid transport system substrate-binding protein	ABC	_13433	urea ABC transporter [Enterobacter ludwigii]	99
04393	F11	glycerol uptake facilitator protein	Major Intrinsic	_00230	aquaporin [Enterobacter ludwigii]	99
04394	F12	glycerol kinase	Glycerol kinase	_00370 _02782	NA	NA
04978	BB11	putative hydroxymethylpyrimidine transport system substrate-binding protein	ABC	_09084	thiamine biosynthesis protein [Enterobacter ludwigii]	97

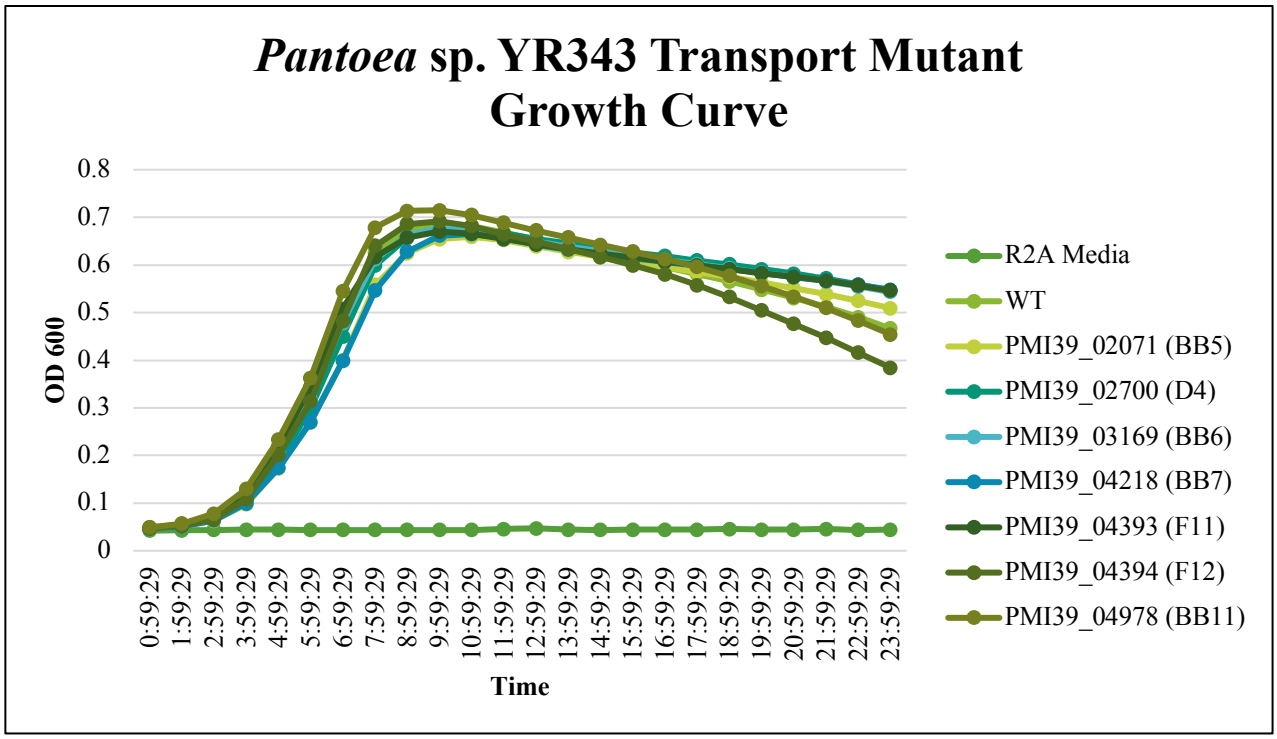


Figure 3.30. Growth curve of transport mutants grown in R2A media.

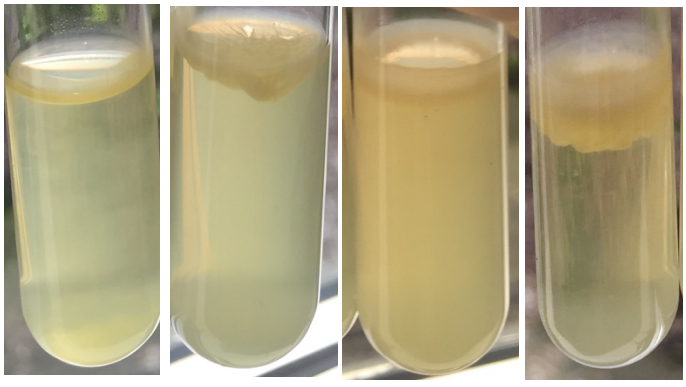


Figure 3.31. Pellicles different from the WT's (right). F11 (left), F12 (second from left), and BB11 (second from right).

Table 3.6. Summary of proteomics for *Pantoea* sp. YR343 transport mutants.

Predicted description	**PMI39_**	**Short ID**	**Log2ratio_GluToSal**
Glycerol kinase	04394	F12	-4.011092507
Glycerol uptake facilitator	04393	F11	-
D-xylose substrate binding	02071	BB5	-4.876327997
Glyceraldehyde 3-phosphate dehydrogenase	03169	BB6	-1.769667321
Substrate-binding ABC	04218	BB7	-
Hydroxymethlypyrmidine substrate-binding	04978	BB11	-0.216521144
L-ribulose-5-phosphate 4-epimerase	02700	D4	-
oligopeptide transport system substrate-binding protein	02667	A9	-1.38225136

Table 3.7. Summary of crytal violet biofilm assay for *Pantoea* sp. YR343 transport mutants.

Predicted description	**PMI39_**	**Short ID**	**550 nm Absorbance**	**Difference from WT**
WT	WT	WT	0.71	0
Glycerol kinase	04394	F12	0.717166667	0.007166667
Glycerol uptake facilitator	04393	F11	0.835	0.125
D-xylose substrate binding	02071	BB5	0.5045	-0.2055
Glyceraldehyde 3-phosphate dehydrogenase	03169	BB6	0.577833333	-0.132166667
Substrate-binding ABC	04218	BB7	0.556166667	-0.153833333
Hydroxymethlypyrmidine substrate-binding	04978	BB11	0.530666667	-0.179333333
L-ribulose-5-phosphate 4-epimerase	02700	D4	0.734333333	0.024333333

LIST OF REFERENCES

1. Bible AN, Fletcher SJ, Pelletier DA, Schadt CW, Jawdy SS, Weston DJ, et al. A Carotenoid-Deficient Mutant in Pantoea sp. YR343, a Bacteria Isolated from the Rhizosphere of Populus deltoides, Is Defective in Root Colonization. Front Microbiol. 2016;7:491.
2. Steeves. Populus deltoides image. 2006.
3. Burke AK, D. A. Duong, R. V. Jensen and A. M. Stevens Analyzing the transcriptomes of two quorum-sensing controlled transcription factors, RcsA and LrhA, important for Pantoea stewartii virulence. PLoS One. 2015;10(12):1-18.
4. Barret M, Morrissey, J. P., & O'Gara, F. Functional genomics analysis of plant growth-promoting rhizobacterial traits involved in rhizosphere competence. Biology and Fertility of Soils. 2011;47(7):729-43.
5. Tecon R, Leveau JH. Symplasmata are a clonal, conditional, and reversible type of bacterial multicellularity. Sci Rep. 2016;6:31914.
6. Fuqua C, Greenberg EP. Listening in on bacteria: acyl-homoserine lactone signalling. Nat Rev Mol Cell Biol. 2002;3(9):685-95.
7. Hengge R. Principles of c-di-GMP signalling in bacteria. Nat Rev Microbiol. 2009;7(4):263-73.
8. Majdalani N, Gottesman S. The Rcs phosphorelay: a complex signal transduction system. Annu Rev Microbiol. 2005;59:379-405.
9. Selin C, de Kievit TR, Belmonte MF, Fernando WG. Elucidating the Role of Effectors in Plant-Fungal Interactions: Progress and Challenges. Front Microbiol. 2016;7:600.
10. Soliveres S, Maestre FT. Plant-plant interactions, environmental gradients and plant diversity: a global synthesis of community-level studies. Perspect Plant Ecol Syst. 2014;16(4):154-63.
11. Glick BR. Plant growth-promoting bacteria: mechanisms and applications. Scientifica (Cairo). 2012;2012:963401.
12. Chisholm ST, Coaker G, Day B, Staskawicz BJ. Host-microbe interactions: shaping the evolution of the plant immune response. Cell. 2006;124(4):803-14.
13. Hahn M, Mendgen K. Signal and nutrient exchange at biotrophic plant-fungus interfaces. Curr Opin Plant Biol. 2001;4(4):322-7.
14. Bakker MG, Schlatter DC, Otto-Hanson L, Kinkel LL. Diffuse symbioses: roles of plant-plant, plant-microbe and microbe-microbe interactions in structuring the soil microbiome. Mol Ecol. 2014;23(6):1571-83.
15. Berendsen RL, Pieterse CM, Bakker PA. The rhizosphere microbiome and plant health. Trends Plant Sci. 2012;17(8):478-86.
16. Turner TR, James EK, Poole PS. The plant microbiome. Genome Biol. 2013;14(6):209.
17. Schmidt J, Fester T, Schulz E, Michalzik B, Buscot F, Gutknecht J. Effects of plant-symbiotic relationships on the living soil microbial community and microbial necromass in a long-term agro-ecosystem. Sci Total Environ. 2017;581-582:756-65.
18. Schlatter DC, Bakker MG, Bradeen JM, Kinkel LL. Plant community richness and microbial interactions structure bacterial communities in soil. Ecology. 2015;96(1):134-42.
19. Gross N, Robson TM, Lavorel S, Albert C, Le Bagousse-Pinguet Y, Guillemin R. Plant response traits mediate the effects of subalpine grasslands on soil moisture. New Phytol. 2008;180(3):652-62.
20. Mendes R, Garbeva P, Raaijmakers JM. The rhizosphere microbiome: significance of plant beneficial, plant pathogenic, and human pathogenic microorganisms. FEMS Microbiol Rev. 2013;37(5):634-63.

21. Zamioudis C, Pieterse CM. Modulation of host immunity by beneficial microbes. Mol Plant Microbe Interact. 2012;25(2):139-50.
22. Beneduzi A, Ambrosini A, Passaglia LM. Plant growth-promoting rhizobacteria (PGPR): Their potential as antagonists and biocontrol agents. Genet Mol Biol. 2012;35(4 (suppl)):1044-51.
23. Bloemberg GV, Lugtenberg BJ. Molecular basis of plant growth promotion and biocontrol by rhizobacteria. Curr Opin Plant Biol. 2001;4(4):343-50.
24. Hayat R, Ali, S., Amara, U., Khalid, R., & Ahmed, I. Soil beneficial bacteria and their role in plant growth promotion: A review. Annu Rev Microbiol. 2010;60(4):579-98.
25. Gottel NR, Castro HF, Kerley M, Yang Z, Pelletier DA, Podar M, et al. Distinct microbial communities within the endosphere and rhizosphere of Populus deltoides roots across contrasting soil types. Appl Environ Microbiol. 2011;77(17):5934-44.
26. Hood EE. Plant-based biofuels. F1000Res. 2016;5.
27. Davis JM. Springer New York; 2008.
28. Shakya M, Gottel N, Castro H, Yang ZK, Gunter L, Labbe J, et al. A multifactor analysis of fungal and bacterial community structure in the root microbiome of mature Populus deltoides trees. PLoS One. 2013;8(10):e76382.
29. Brady C, Cleenwerck I, Venter S, Vancanneyt M, Swings J, Coutinho T. Phylogeny and identification of Pantoea species associated with plants, humans and the natural environment based on multilocus sequence analysis (MLSA). Syst Appl Microbiol. 2008;31(6-8):447-60.
30. Walterson AM, & Stavrinides, J. Pantoea: insights into a highly versatile and diverse genus within Enterobacteriaceae. FEMS Microbiol Rev. 2015;39(6):968-84.
31. Nadarasah G, Stavrinides J. Quantitative evaluation of the host-colonizing capabilities of the enteric bacterium Pantoea using plant and insect hosts. Microbiology. 2014;160(Pt 3):602-15.
32. Polisetti S, Bible AN, Morrell-Falvey JL, Bohn PW. Raman chemical imaging of the rhizosphere bacterium Pantoea sp. YR343 and its co-culture with Arabidopsis thaliana. The Analyst. 2016;141(7):2175-82.
33. . !!! INVALID CITATION !!! 5, 33.
34. Hosni T, Moretti, C., Devescovi, G., Suarez-Moreno, Z. R., Fatmi, M. B., Guarnaccia, C., and , Venturi V. Sharing of quorum-sensing signals and role of interspecies communities in a bacterial plant disease. ISME J. 2011;5(12):1857-70.
35. Andersen JB, Heydorn A, Hentzer M, Eberl L, Geisenberger O, Christensen BB, et al. gfp-based N-acyl homoserine-lactone sensor systems for detection of bacterial communication. Appl Environ Microbiol. 2001;67(2):575-85.
36. Pratt LA, Kolter R. Genetic analysis of Escherichia coli biofilm formation: roles of flagella, motility, chemotaxis and type I pili. Mol Microbiol. 1998;30(2):285-93.
37. O'Toole GA, Wong GC. Sensational biofilms: surface sensing in bacteria. Curr Opin Microbiol. 2016;30:139-46.
38. Belas R. Biofilms, flagella, and mechanosensing of surfaces by bacteria. Trends in microbiology. 2014;22(9):517-27.
39. Mah TFC, O'Toole GA. Mechanisms of biofilm resistance to antimicrobial agents. Trends Microbiol. 2001;9(1):34-9.
40. Yang L, Liu Y, Wu H, Song Z, Hoiby N, Molin S, et al. Combating biofilms. FEMS Immunol Med Microbiol. 2012;65(2):146-57.
41. Barraud N, Kelso MJ, Rice SA, Kjelleberg S. Nitric oxide: a key mediator of biofilm dispersal with applications in infectious diseases. Curr Pharm Des. 2015;21(1):31-42.

42. O'Toole GA, Kolter R. Flagellar and twitching motility are necessary for Pseudomonas aeruginosa biofilm development. Mol Microbiol. 1998;30(2):295-304.
43. Ren GX, Fan S, Guo XP, Chen SY, Sun YC. Differential Regulation of c-di-GMP Metabolic Enzymes by Environmental Signals Modulates Biofilm Formation in Yersinia pestis. Front Microbiol. 2016;7.
44. Christensen LD, van Gennip M, Rybtke MT, Wu H, Chiang WC, Alhede M, et al. Clearance of Pseudomonas aeruginosa foreign-body biofilm infections through reduction of the cyclic Di-GMP level in the bacteria. Infect Immun. 2013;81(8):2705-13.
45. Romling U, Galperin MY, Gomelsky M. Cyclic di-GMP: the First 25 Years of a Universal Bacterial Second Messenger. Microbiol Mol Biol R. 2013;77(1):1-52.
46. Perez-Mendoza D, Aragon IM, Prada-Ramirez HA, Romero-Jimenez L, Ramos C, Gallegos MT, et al. Responses to elevated c-di-GMP levels in mutualistic and pathogenic plant-interacting bacteria. PLoS One. 2014;9(3):e91645.
47. Politis DJ, Goodman RN. Fine Structure of Extracellular Polysaccharide of Erwinia amylovora. Appl Environ Microbiol. 1980;40(3):596-607.
48. Bernhard F, Schullerus D, Bellemann P, Nimtz M, Coplin DL, Geider K. Genetic transfer of amylovoran and stewartan synthesis between Erwinia amylovora and Erwinia stewartii. Microbiology. 1996;142 (Pt 5):1087-96.
49. Ayers AR, Ayers SB, Goodman RN. Extracellular Polysaccharide of Erwinia amylovora: a Correlation with Virulence. Appl Environ Microbiol. 1979;38(4):659-66.
50. Dolph PJ, Majerczak DR, Coplin DL. Characterization of a gene cluster for exopolysaccharide biosynthesis and virulence in Erwinia stewartii. J Bacteriol. 1988;170(2):865-71.
51. Amellal N, Burtin G, Bartoli F, Heulin T. Colonization of wheat roots by an exopolysaccharide-producing pantoea agglomerans strain and its effect on rhizosphere soil aggregation. Appl Environ Microbiol. 1998;64(10):3740-7.
52. Vande Broek A, Lambrecht, M., & Vanderleyden, J. Bacterial chemotactic motility is important for the initiation of wheat root colonization by Azospirillum brasilense. Microbiology. 1998;144(9):2599-606.
53. Langlotz T, Degendorfer C, Mulloni A, Schall G, Reitmayr G, Schmalstieg D. Robust detection and tracking of annotations for outdoor augmented reality browsing. Comput Graph. 2011;35(4):831-40.
54. Nimtz M, Mort A, Wray V, Domke T, Zhang Y, Coplin DL, et al. Structure of stewartan, the capsular exopolysaccharide from the corn pathogen Erwinia stewartii. Carbohydrate research. 1996;288:189-201.
55. Koutsoudis MD, Tsaltas D, Minogue TD, von Bodman SB. Quorum-sensing regulation governs bacterial adhesion, biofilm development, and host colonization in Pantoea stewartii subspecies stewartii. Proc Natl Acad Sci U S A. 2006;103(15):5983-8.
56. Stout V, Torres-Cabassa A, Maurizi MR, Gutnick D, Gottesman S. RcsA, an unstable positive regulator of capsular polysaccharide synthesis. J Bacteriol. 1991;173(5):1738-47.
57. Pristovsek P, Sengupta K, Lohr F, Schafer B, von Trebra MW, Ruterjans H, et al. Structural analysis of the DNA-binding domain of the Erwinia amylovora RcsB protein and its interaction with the RcsAB box. J Biol Chem. 2003;278(20):17752-9.
58. Wehland M, Bernhard F. The RcsAB box. Characterization of a new operator essential for the regulation of exopolysaccharide biosynthesis in enteric bacteria. J Biol Chem. 2000;275(10):7013-20.

59. Ramachandran R, Burke AK, Cormier G, Jensen RV, Stevens AM. Transcriptome-based analysis of the Pantoea stewartii quorum-sensing regulon and identification of EsaR direct targets. Appl Environ Microbiol. 2014;80(18):5790-800.
60. Minogue TD, Wehland-von Trebra M, Bernhard F, von Bodman SB. The autoregulatory role of EsaR, a quorum-sensing regulator in Pantoea stewartii ssp. stewartii: evidence for a repressor function. Mol Microbiol. 2002;44(6):1625-35.
61. Chen Y, Lv M, Liao L, Gu Y, Liang Z, Shi Z, et al. Genetic Modulation of c-di-GMP Turnover Affects Multiple Virulence Traits and Bacterial Virulence in Rice Pathogen Dickeya zeae. PLoS One. 2016;11(11):e0165979.
62. O'Toole GA, Kolter R. Initiation of biofilm formation in Pseudomonas fluorescens WCS365 proceeds via multiple, convergent signalling pathways: a genetic analysis. Mol Microbiol. 1998;28(3):449-61.
63. Khan SR, Gaines J, Roop RM, 2nd, Farrand SK. Broad-host-range expression vectors with tightly regulated promoters and their use to examine the influence of TraR and TraM expression on Ti plasmid quorum sensing. Appl Environ Microbiol. 2008;74(16):5053-62.
64. Islam ST, Lam JS. Wzx flippase-mediated membrane translocation of sugar polymer precursors in bacteria. Environ Microbiol. 2013;15(4):1001-15.
65. Bernhard F, Coplin DL, Geider K. A gene cluster for amylovoran synthesis in Erwinia amylovora: characterization and relationship to cps genes in Erwinia stewartii. Molecular & general genetics : MGG. 1993;239(1-2):158-68.
66. Fraser GM, Hughes C. Swarming motility. Curr Opin Microbiol. 1999;2(6):630-5.
67. Kearns DB. A field guide to bacterial swarming motility. Nat Rev Microbiol. 2010;8(9):634-44.
68. Alavi M, Belas R. Surface sensing, swarmer cell differentiation, and biofilm development. Methods Enzymol. 2001;336:29-40.
69. Schafer A, Tauch A, Jager W, Kalinowski J, Thierbach G, Puhler A. Small mobilizable multi-purpose cloning vectors derived from the Escherichia coli plasmids pK18 and pK19: selection of defined deletions in the chromosome of Corynebacterium glutamicum. Gene. 1994;145(1):69-73.

APPENDIX

In order to develop chromosomal deletions of *rcsA* and *lrhA* to use for transcriptome and functional analyses, we inserted two 1 kb base pair fragments from upstream and downstream of the gene of interest into the modified pk18*mobsac*B vector (Figure A.1). After confirming the insertion via PCR and gel electrophoresis, we electroporated the plasmids into *Pantoea* sp. YR343.

We began screening using antibiotic selectors to ensure the plasmid was present. We then attempted to kick out the plasmid backbone with sucrose, because the modified pk18 plasmid has a *sacB* gene that expresses levansucrase, which is lethal for cells in the presence of sucrose.[69] Then, we had an additional selection for Δ*rcsA* candidates based on the strong trypan blue phenotype of the transposon mutants (Figure A.2-A.3). The selected deletion strains will be screened with PCR using primers for *rcsA* corresponding to upstream, downstream, and inside the gene. DNA sequencing of the selected PCR products will confirm the deletion strain.

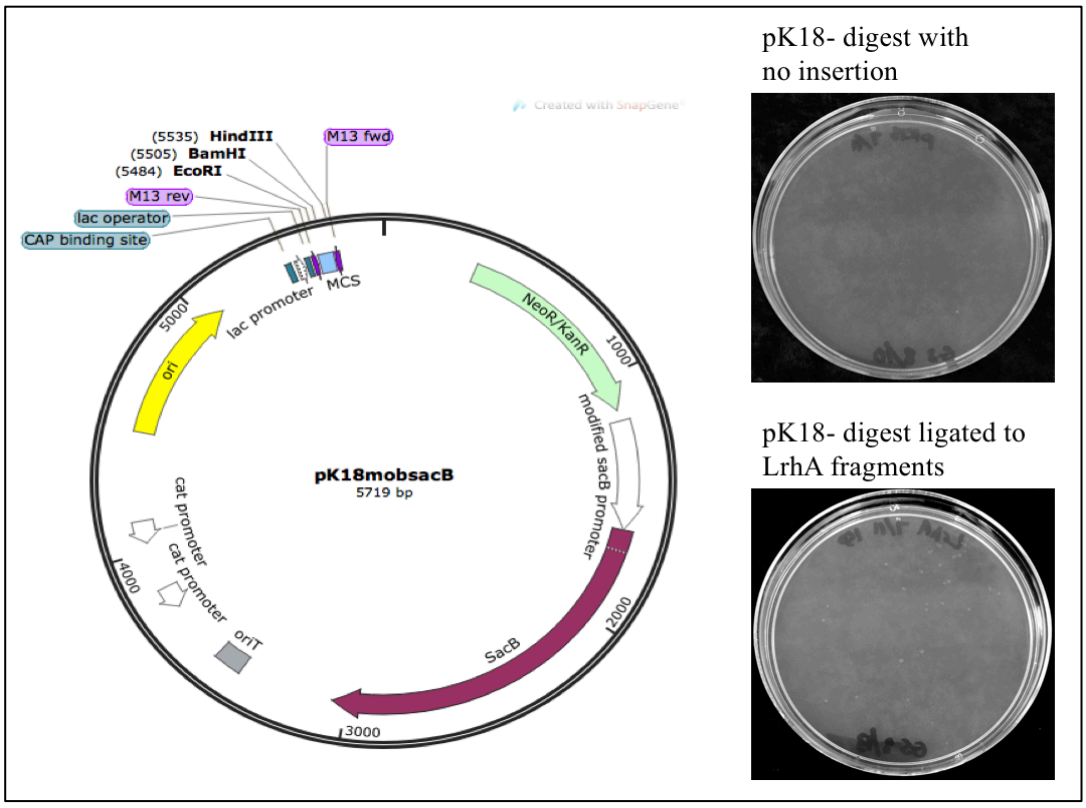


Figure A.1. Modified pk18mobsacB plasmid (left). Transformation of the plasmid with no insertion (top right) and with insertion (bottom left).

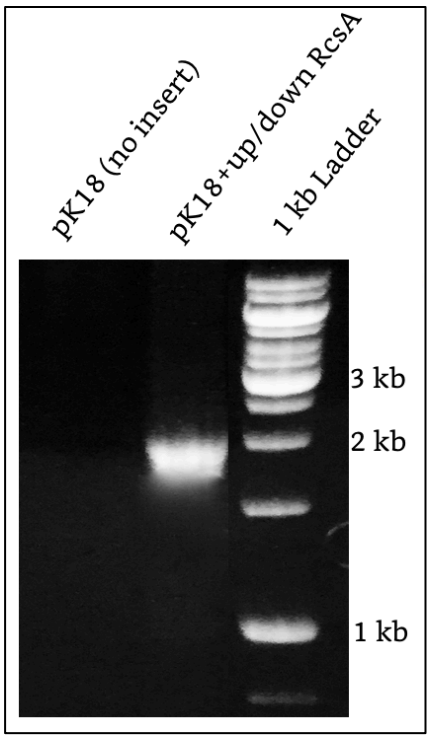


Figure A.2. Gel electrophoresis showing presence of *rcsA* insert into pk18mobsacB plasmid.

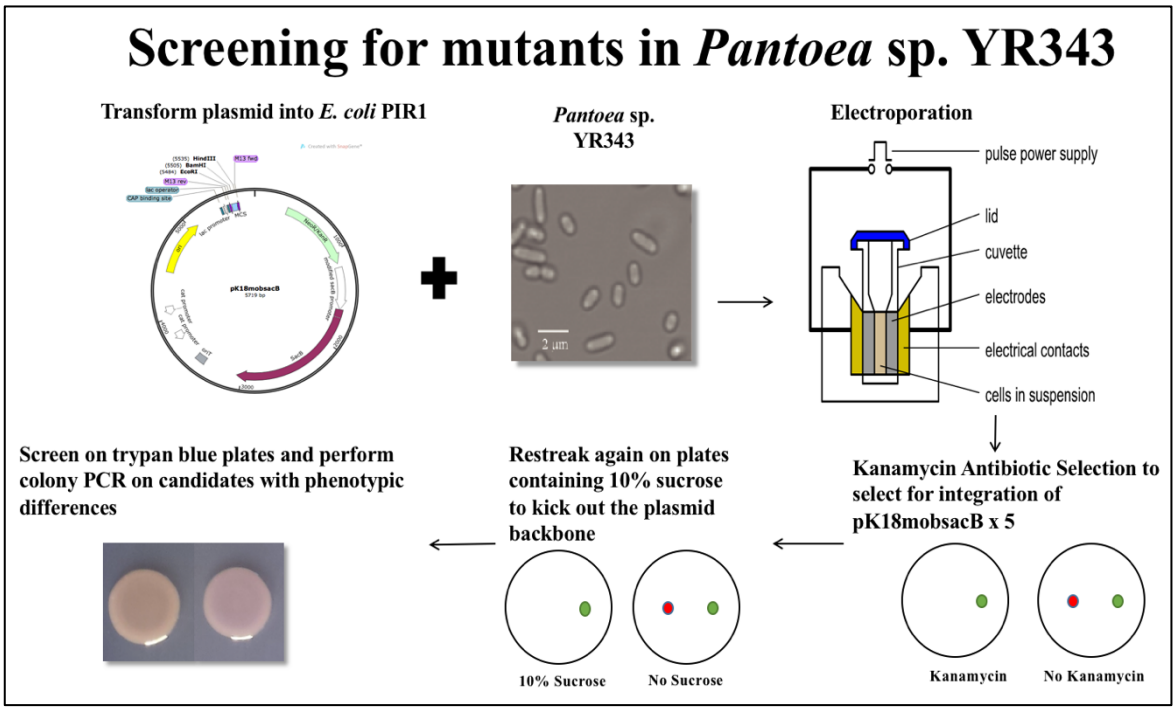


Figure A.3. Diagram of screen for *rcsA* clean deletion mutant.

Table A.1. Primers.

Primer	**Sequence**	**Cutting Enzyme**	**Annealing Tempera-ture (C)**	**Location**
LrhA_upFor_EcoRI	GCATTGAATTCAGC TTGCCGGATTTATC	EcoRI	52	Upstream, top strand, 1000 bp from *lrhA*
LrhA_upRev_BamHI	GATGGATCCCGAT TTGCATTAGTCATG	BamHI	49	Upstream, bottom strand, overlapping *lrhA*
LrhA_downFor_BamHI	TAGGGATCCAGTA GGGGTTACAGTTGC	BamHI	54	Downstream, top strand, overlapping *lrhA*
LrhA_downRev_HindIII	AAGAAGCTTGCCA AGAGCACCAAAATG	HindIII	56	Downstream, bottom strand, 1000 bp from *lrhA*
RcsA_upFor_EcoRI	ATTGCGAATTCAAC GGACATCTGTGGCTG	EcoRI	54	Upstream, top strand, 1000 bp from *rcsA*
RcsA_upRev_BamHI	TTGGGATCCTTG GCATTATAGCGACCC	BamHI	52	Upstream, bottom strand, overlapping *rcsA*
RcsA_downFor_BamHI	AAGGGATCCTCAG TGAATAAAGGGGCC	BamHI	52	Downstream, top strand, overlapping *rcsA*
RcsA_downRev_HindIII	AAGAAGCTTTTCA CGCACCGTTCCTAC	HindIII	55	Downstream, bottom strand, 1000 bp from *rcsA*

Table A.1 Continued. Primers.

Primer	**Sequence**	**Cutting Enzyme**	**Annealing Tempera-ture (C)**	**Location**
LrhA_out_For	TTGCCGATGTTC AGCTTG		55	1100 bp upstream of *lrhA,* top strand
LrhA_out_Rev	TGCTTATGAGGG TTGGTG		54	1100 bp downstream of *lrhA,* bottom strand
RcsA_out_For	GTGCTGGCACGT TTTCTC		55	1100 bp upstream of *rcsA,* top strand
RcsA_out_Rev	AGCTTGCTCTTC AGTACG		54	1100 bp downstream of *rcsA,* bottom strand

VITA

Grace Satterfield graduated from Samford University in May of 2015 with a Bachelors of Arts and Sciences in Biology and History. She attended the University of Tennessee, Knoxville, in August of that year to join the Genome Science and Technology graduate program with a major in Life Sciences. During her graduate work, she conducted research as part of the Plant-Microbe Interactions group at Oak Ridge National Lab under the supervision of Dr. Jennifer Morrell-Falvey.